A multivalent adaptor mechanism drives the nuclear import of proteasomes

Hanna L. Brunner[1,2], Robert W. Kalis[1,2,6], Lorenz Grundmann[1,2,6], Zuzana Hodáková[1], Zuzana Koskova[3], Irina Grishkovskaya[1], Melanie de Almeida[1], Matthias Hinterndorfer[1], Simon Höfflin[1], Florian Andersch[1], Harald Kotisch[1], Achim Dickmanns[4], Sara Cuylen-Häring[3], Johannes Zuber[1,5,*] & David Haselbach[1,*]

Abstract

Nuclear protein homeostasis, including the turnover of transcription factors, critically depends on nuclear proteasomes. After each cell division, proteasomes need to be re-imported into the newly formed nucleus in a highly dynamic process that requires the largely unstructured protein AKIRIN2. However, how AKIRIN2 orchestrates this process and, more generally, how large protein complexes are translocated into the nucleus remains poorly understood. Here, we have used an integrated approach combining protein-wide saturation mutagenesis screens, cryoEM, and biochemical reconstitution to characterize AKIRIN2 as a scaffold protein that coordinates the stepwise assembly of an importin cluster around the proteasome. Through surveying every possible single amino acid substitution in AKIRIN2 using FACS- and microscopy-based genetic screens, we establish a comprehensive map of functionally relevant residues and binding interfaces in structured and disordered protein regions. Integrating these results with cryoEM analysis reveals a wing helix in a disordered region of AKIRIN2 that plays a crucial role in stabilizing proteasome interactions. Upon primary binding, AKIRIN2 homodimers recruit the importin IPO9, which in turn facilitates the binding of a second AKIRIN2 homodimer that recruits additional importins. Together, this multivalent molecular assembly amplifies the number of nuclear localisation signals and, thereby, triggers efficient proteasome translocation into the nucleus. Inside the nucleus, RanGTP rapidly dissociates importins, and AKIRIN2 is degraded by the proteasome in a ubiquitin-independent manner. Beyond mechanistically resolving the nuclear import of proteasomes, we propose that multivalent adaptor proteins like AKIRIN2 orchestrate the import of other macromolecular complexes and thereby dynamically control the composition of the nuclear proteome.

Thousands of proteins shuttle between the cyto- and nucleoplasm. This process is controlled by the nuclear pore complex (NPC), which acts as a selective gateway for nucleocytoplasmic transport. Current models of nuclear import describe how importin-β family proteins recognize motifs such as nuclear localisation signals (NLS) on cargo proteins and facilitate their passage through the NPC.[1,2] However, the mechanism by which large assemblies and complexes efficiently traverse the NPC to enter the nucleus is more intricate. While studies on viral particle entry suggest that cargo size correlates with the number of importins required for effective import, this phenomenon is unexplored for endogenous complexes[3,4].

Large complexes with critical nuclear functions include the proteasome, which is essential for nuclear protein homeostasis and the regulation of fundamental processes such as the cell cycle and transcription. Despite the high abundance of proteasomes in the nucleus, mechanisms governing their import have long remained elusive in higher organisms.[5–7] We recently uncovered AKIRIN2, a highly conserved and essential protein, as a key factor in this process[8]. Cells dividing in the absence of AKIRIN2 fail to re-import proteasomes into the nucleus. Consequently, nuclear factors accumulate, and cells rapidly undergo apoptotic cell death, demonstrating that AKIRIN2 is strictly required for nuclear proteasome import. However, how this small protein mediates the import of these large protein complexes has remained elusive.

[1]Research Institute of Molecular Pathology (IMP), Vienna BioCenter (VBC), Campus-Vienna-Biocenter 1, 1030, Vienna, Austria. [2]Vienna BioCenter PhD Program, Doctoral School of the University of Vienna and Medical University of Vienna, 1030, Vienna, Austria. [3]European Molecular Biology Laboratory (EMBL) Heidelberg. [4]Department of Molecular Structural Biology, Institute of Microbiology and Genetics, GZMB, Georg-August-University Göttingen, Justus-von-Liebig-Weg 11, 37077 Göttingen, Germany. [5]Medical University of Vienna, VBC, Vienna, Austria. [6]These authors contributed equally: Robert Kalis and Lorenz Grundmann. [*]Corresponding authors: johannes.zuber@imp.ac.at & david.haselbach@imp.ac.at

Saturation mutagenesis screens identify functionally relevant features of AKIRIN2

Human AKIRIN2 was found to directly interact with mature 20S and 26S proteasome particles via a conserved SYVS motif. Further, it contains a bipartite classical nuclear localisation sequence (cNLS) and a C-terminal coiled-coil dimerization domain[8]. While our prior structural work provided insights into interactions between AKIRIN2 and the proteasome, 76% remained structurally unresolved due to its flexible nature (Fig. 1a). To gain insights into molecular functions and underlying features of AKIRIN2, we devised a series of saturation mutagenesis screens (SMScreens) in which we systematically probed the functional relevance of each amino acid for nuclear proteasome import. To this end, we constructed a lentiviral cDNA library containing 4,500 AKIRIN2 variants harbouring a specific mutation that either deletes a specific codon or converts it into an optimized codon of any possible amino acid or a STOP codon.

To quantify the impact of these variants on nuclear proteasome import, we engineered iCas9.RKO cells[8] to express two complimentary reporter alleles. First, we replaced an endogenous subunit of the 20S proteasome with a fluorescently tagged version (PSMB4-StayGold) to enable the monitoring of proteasome localisation through live-cell microscopy. Second, we stably expressed an mCherry-MYC fusion protein serving as a highly dynamic reporter of nuclear proteasome activity[8]. In addition, we stably expressed a pair of sgRNAs targeting AKIRIN2, which together with doxycycline (dox)-inducible Cas9 (iCas9) enable efficient, temporally controlled knockout of endogenous AKIRIN2 (Fig. 1b, Extended Data Fig. 1a,b). Following cDNA library transduction, selection, and dox-induced depletion of endogenous AKIRIN2, we quantified rescue effects mediated by sgRNA-resistant AKIRIN2 variants contained in our library using three complementary high-throughput assays: (I) Using fluorescence-activated cell sorting (FACS), we isolated cells displaying elevated mCherry-MYC levels, indicating dysfunctional proteasome import. (II) We employed a prototype of a high-speed image-enabled cell sorting device[9] to isolate cells displaying reduced nuclear proteasome content based on our PSMB4-StayGold reporter. (III) Since AKIRIN2 is strictly essential for cell survival, we also performed a proliferation-based screen, where cells expressing dysfunctional AKIRIN2 variants are expected to drop out over time. In all three screens, we quantified the relative representation of each AKIRIN2 variant using next-generation sequencing of cDNA cassettes PCR-amplified from genomic DNA of sampled cells (Fig. 1b).

Despite differences in dynamic range and resolution, all three screening approaches yielded highly consistent results and reliably detected functionally relevant features of AKIRIN2. A merged analysis of the data from all screens (Fig. 1c,d, Extended Data Fig. 1c,d) shows that, in line with the critical role of the C-terminal SYVS-motif for proteasome binding, all STOP-variants and mutations within YVS were identified as dysfunctional, while amino acid self-replacements with alternative codons remained broadly neutral. Similarly, our screens confirmed the critical role of the N-terminal bipartite cNLS. Moreover, deletions or helix-breaking prolines within the coiled-coil domain (residues 142-190) were detrimental to AKIRIN2 function, likely due to the disruption of the domain's essential role in homodimerization. Specific residues mediating key interactions between two AKIRIN2 protomers (A and B) included $C152^A$:$C152^B$ (disulfide bond), $R159^A$:$E160^B$, $E160^A$:$R159^B$, $Y167^A$:$Y167^B$ (π-π), $L171^A$:$L171^B$, and $F182^A$:$F185^B$ (π-π) (Fig. 1c,d). In addition, our SMScreens revealed several previously unknown functionally relevant regions. For example, we identified a crucial domain containing indispensable residues (E79, I85, K94), which we termed the wing helix (residues 78-101). Deletion of this helix severely impaired AKIRIN2 function, suggesting its importance in protein-protein interactions or regulatory roles (Fig. 1c,d, Extended Data Fig. 2a-c). Moreover, we detected a striking intolerance to mutations at residue D188 (Extended Data Fig. 2a-c), hinting at a critical, yet undefined function. This residue does not appear to be involved in dimerization or proteasome binding, suggesting a role in interactions with other factors.

Our SMScreens reveal a detailed functional map of AKIRIN2, uncovering numerous critical interaction sites beyond its established NLS and proteasome-binding motifs, suggesting that previously unrecognized residues may serve as regulatory, or interaction points involved in coordinating the proteasome and nuclear import machinery.

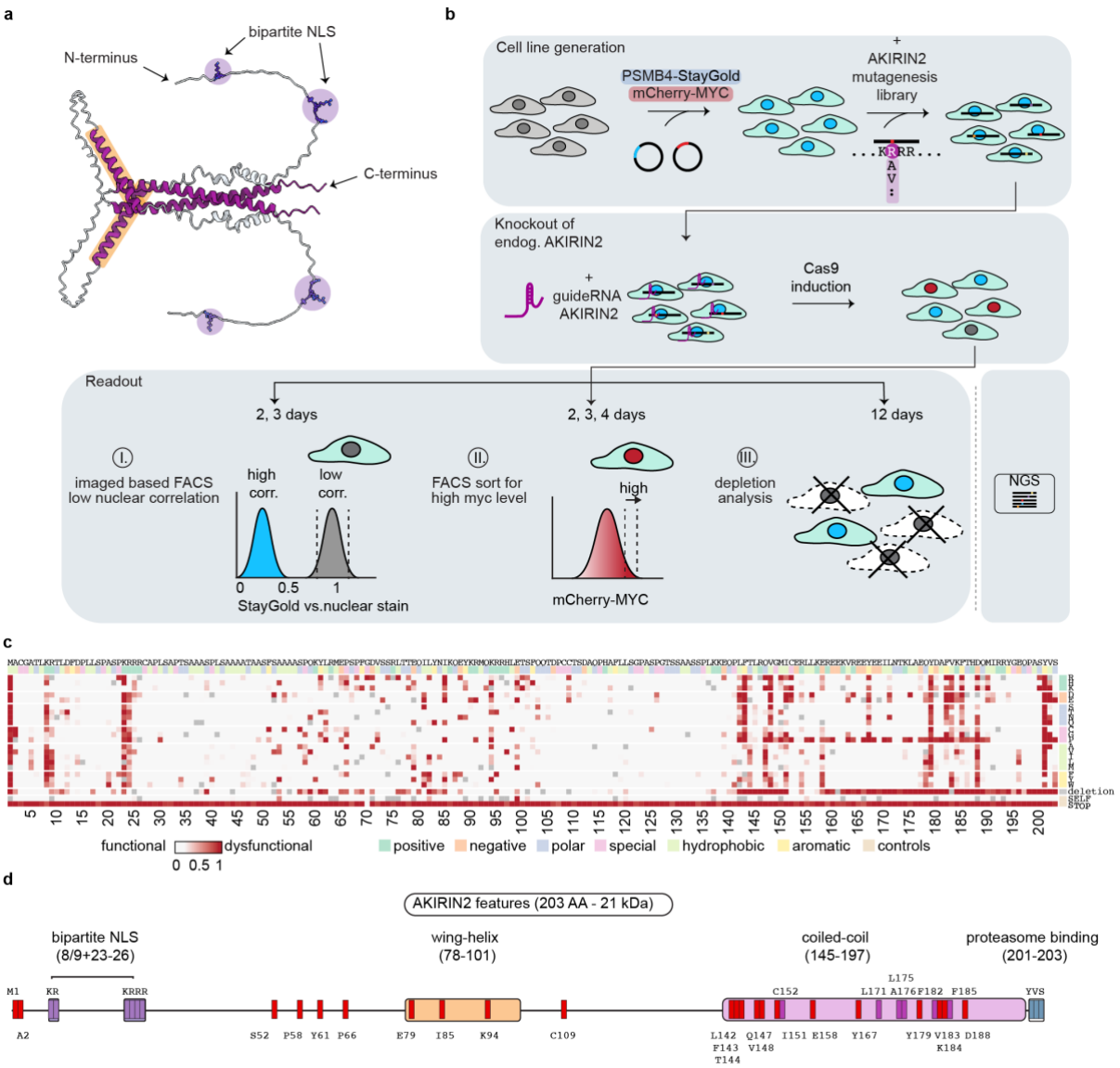

Fig. 1 | Saturation mutagenesis screens (SMScreens) map functional importance of AKIRIN2 residues. a, AlphaFold3 predicted a dimeric structure of AKIRIN2 showing the coiled-coil dimerization domain (dark pink), wing α-helices (dark pink highlighted with orange) and the bipartite cNLSs (purple). **b**, Schematic representation of the generation of the 20S reporter cell line expressing StayGold-labelled proteasomes and mCherry-MYC, transduced with an AKIRIN2 mutagenesis library and a dsgAKIRIN2 for the knockout of endogenous AKIRIN2. Followed by a schematic workflow of the screen starting with Cas9 induction for 2-4 days before sorting either for: I. low-correlation between nuclear staining and StayGold-proteasome or, II. high mCherry levels, additionally III. long-term dropout cells are analysed. Subsequently all samples are sent for NGS to quantify mutants. **c**, Heat plot representing cumulative analysis of the SMScreens results, showing dysfunctional mutations in red shades. **d**, Schematic representation of AKIRIN2 features, coloured as in (**a**). Residues that emerged to be crucial but with unassigned function are marked with a red square, residues that were assigned to be important for dimerization by AF3 predictions or cryoEM structure are marked with a purple square, blue squares mark residues known to be essential for proteasome binding, dark purple squares mark the bipartite cNLS.

IPO9 is a key component of AKIRIN2-mediated proteasome nuclear import

We previously demonstrated that AKIRIN2 interacts with several importins and therefore sought to identify additional proteins involved in AKIRIN2-mediated nuclear import. Knockout of KPNA2 or KPNB1 did not affect nuclear proteasome localisation (Fig. 2a, Extended Data Fig. 3a). However, the redundancy among the six human importin-αs suggests functional compensation among these proteins. In the case of KPNB1, crucial for many canonical import processes, its knockout led to increased MYC levels and rapid cell death before mitosis could even occur. Most promising was the deletion of IPO9 which resulted in a phenotype similar to AKIRIN2 (Fig. 2a, Extended Data Fig. 3a) knockout, though with a

delayed onset. To investigate this further, we focused on potential interactions with IPO9. Co-immunoprecipitation coupled with mass spectrometry (Co-IP/MS) identified AKIRIN2 as one of the most enriched interactors of IPO9 (Fig. 2b), along with known partners like Ran and histones H2A/H2B. These results suggest that IPO9 is a major, though not exclusive, component of the proteasomal import pathway.

We next examined direct interactions between 20S proteasome, AKIRIN2, and IPO9 using *in vitro* reconstitution in sucrose density gradients (Fig. 2c, Extended Data Fig. 3b). We focused here on 20S proteasomes to reduce the complexity. IPO9 alone failed to bind the proteasome, but addition of AKIRIN2 led to formation of a ternary complex (Fig. 2d, Extended Data Fig. 3b-d). Additionally, we observed the formation of binary AKIRIN2-IPO9 complexes with a fraction that tends to precipitate hinting towards oligomerisation of the proteins (Extended Data Fig. 3c). AKIRIN2 alone was distributed across multiple gradient fractions indicating the formation of higher oligomers. Quantitative binding assays revealed a low µM binding affinity for AKIRIN2-proteasome and a higher affinity interaction between AKIRIN2 and IPO9 (KD ≈ 40 nM) (Extended Data Fig. 3e,f). These findings establish AKIRIN2 as a crucial adaptor that anchors IPO9 to the proteasome, forming a key component of the nuclear import complex. The ability of AKIRIN2 to form both binary and ternary complexes suggests a stepwise assembly mechanism for proteasome nuclear import.

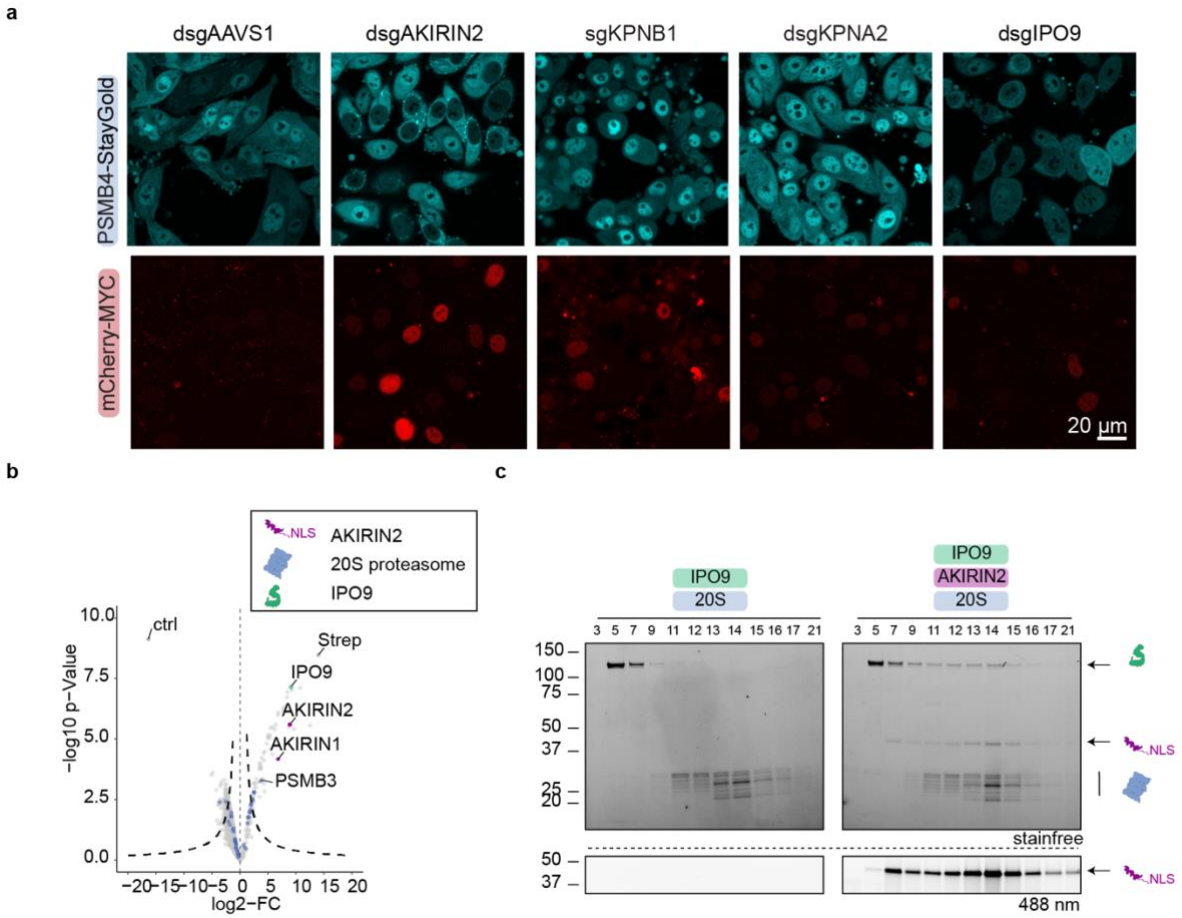

Fig. 2 | Importin IPO9 engages proteasomes via AKIRIN2. a, Representative confocal image (scale bar: 20 µm) of StayGold-PSMB4 RKO reporter cell line showing localisation of proteasomes as well as mCherry-MYC after 2- or 5-days knockout induction (depending on protein half-life) of AAVS1 (2 d), AKIRIN2 (2 d), KPNA2 (5 d), KPNB1 (5 d) or IPO9 (5 d). **b**, Volcano plot of Co-IP/MS of Strep-tagged-IPO9 in HeLa extract. **c**, SDS-PAGE gel of 10-30% sucrose density gradient of proteasomes with IPO9 in the presence or absence of AKIRIN2.

Structural basis of AKIRIN2-mediated proteasome-importin assembly

To elucidate the molecular architecture of the reconstituted 20S:AKIRIN2:IPO9 complex, we performed electron cryo microscopy (cryoEM), focusing on particles with additional density compared to 20S:AKIRIN2 (pdb: 7NHT) alone. The resulting 3.4 Å resolution map (Extended Data Fig. 4, Extended Data Fig. 5a-e) revealed an unexpected arrangement: two AKIRIN2 dimers (I and II) and one IPO9 molecule bound to the same side of the 20S proteasome (Fig. 3a-c). IPO9 adopts its characteristic HEAT repeat solenoid structure, but interestingly engages AKIRIN2 through a unique interface suggesting AKIRIN2 is not a classical cargo. The C-terminal HEAT repeats H17-H18 bind the coiled-coil of AKIRIN2 dimer I on the outer surface of IPO9's concave structure (Fig. 3a,d) mediated by several residues identified in our SMScreens as crucial (Q178, Y179, F182, V183, F185, D188, M191). This binding mode contrasts with interactions of IPO9 with other known partners like H2A/H2B or RanGTP, which bind the inner concave surface[10].

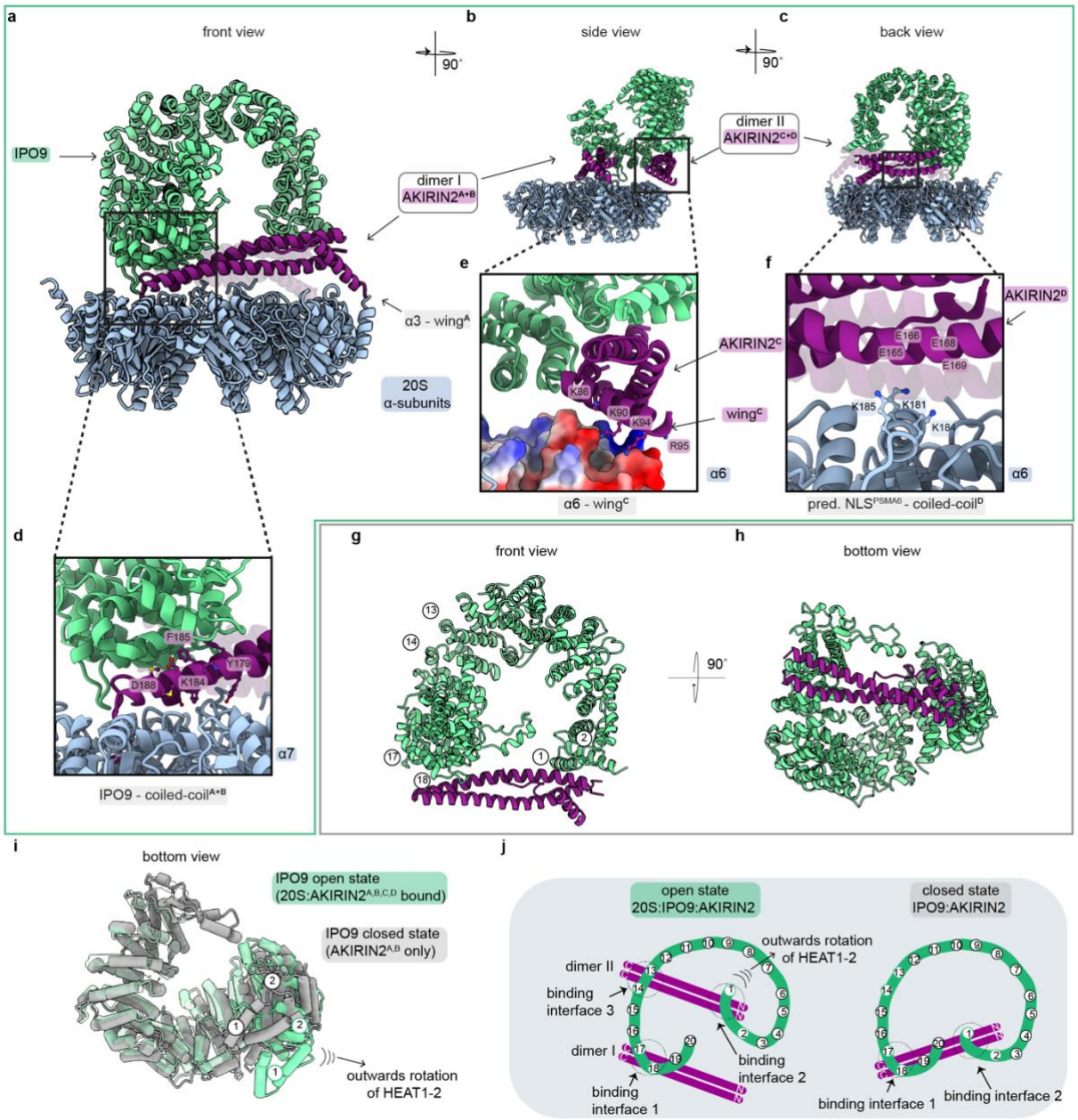

Fig. 3 | Structure of the 20S:AKIRIN2:IPO9 ternary complex reveals clustering of AKIRIN2 on the proteasome. **a-c**, Model of the ternary complex 20S (blue), AKIRIN2 (dark pink) and IPO9 (green) in (**a**) front (**b**) side and (**c**) back view. **d**, Close-up of binding interface of IPO9 with AKIRIN2 dimer I. **e**, Close-up of binding interface with AKIRIN2 dimer II with IPO9 as well as α6 (visualized with its electrostatic surface). **f**, Close-up of four Glutamate acid residues of AKIRIN2 protomer D in the coiled-coil domain which are in close proximity to three Lysin residues of α6. **g-h**, Model of the binary IPO9:AKIRIN2 complex in (**g**) front and (**h**) bottom view. **i**, Overlay of IPO9 in the open (20S:AKIRIN2 bound, green) and closed (AKIRIN2 bound, grey) state, visualizing the rotation of HEAT1-2. **j**, Schematic representation of the IPO9:AKIRIN2 interaction in complex with the proteasome, showing dimer I interacts with its C-terminal end of the coiled-coil with HEAT H17-18, and dimer II interacts with its N-terminal end of the coiled-coil with HEAT H1 and with its C-terminal end of the coiled-coil with HEAT H13-14 (left), schematic representation of the IPO9:AKIRIN2 interaction, showing two binding interfaces between the C-terminal end of the coiled-coil of the AKIRIN2 dimer and HEAT17-18 of IPO9, and it's N-terminal end of the coiled-coil with HEAT H1 (right).

Although IPO9 binding does not significantly alter the interaction of AKIRIN2 dimer I with the proteasome, we can now resolve the wing helix of protomer AKIRIN2^{A}. This reveals additional contacts, particularly the functional important residue K94, which binds to a negatively charged pocket at the C-terminal end of the α3 subunit. This new identified binding interface likely stabilizes the interaction with the proteasome.

The coiled-coil of AKIRIN2 dimer II is sandwiched between IPO9 and the proteasome, with its N-terminal part contacting IPO9's HEAT repeat H1 and its C-terminus engaging HEAT repeats H13-14 (Fig. 3b,c). Notably, we resolved the wing helix of AKIRIN2^{C} where a basic patch (aa: 86-95) interacts with the negatively charged surface of α6 (Fig. 3e). Again, the crucial residue K94 appears to be important for this interaction. Lastly, despite the limited resolution in this region, three glutamate residues (E165, E166, E169) on AKIRIN2^{D} are positioned near a putative NLS (K181, K184, K185) of α6[11], suggesting potential salt bridge formation (Fig. 3f). This interaction may explain the previously described[11] crucial role of this motif in nuclear localisation of the proteasome, although direct interactions with importins were not detected. Strikingly, mapping the SMScreen results onto our ternary complex structure shows that functionally crucial residues cluster at the interaction interfaces with IPO9 and the 20S proteasome (Supplementary video 1). Our structure reveals at least four AKIRIN2 molecules bound to one side of the 20S proteasome, suggesting that AKIRIN2 can simultaneously recruit multiple importins, facilitating transport through their accumulation. These findings demonstrate that AKIRIN2 functions as a multivalent adaptor, nucleating the assembly of a large nuclear import complex through specific protein-protein interactions.

Conformational plasticity underpins AKIRIN2-mediated complex assembly

The observed clustering of AKIRIN2 on the proteasome in the presence of IPO9 prompted us to investigate whether this arrangement is specific to the ternary complex or a general feature of AKIRIN2-IPO9 interactions. We determined the structure of the AKIRIN2-IPO9 binary complex at 3.8 Å resolution, revealing a strikingly different binding mode compared to the ternary complex (Fig. 3g,h and Extended Data Fig. 6a-d). In the binary complex, a single AKIRIN2 dimer bridges the N- and C-terminal domains of IPO9 through two binding sites (Fig. 3h). This interaction compacts IPO9's solenoid structure, rotating HEAT repeats H1-2 inwards to a closed state (Fig. 3i,j, Supplementary video 2). The transition to the ternary complex involves major conformational changes: HEAT repeats H17-H18 maintain an association with AKIRIN2 dimer I, while H1-2 open to accommodate dimer II, which also contacts HEAT repeats H13-14 (Fig. 3j). These rearrangements, stabilized by association with the proteasome, reveal at least three distinct AKIRIN2 binding sites on IPO9. The intrinsic flexibility of both proteins likely facilitates this binding plasticity, enabling the transition from one to two AKIRIN2 dimers in the ternary complex. Functionally, this reconfiguration significantly increases the number of NLSs exposed on the proteasomal cargo, potentially enhancing import efficiency. This structural plasticity illuminates a dynamic assembly mechanism for large nuclear import complexes, balancing adaptable cargo recognition with efficient nuclear pore translocation.

AKIRIN2 recruits multiple importin types for efficient proteasome import

Our SMScreens confirmed the critical role of AKIRIN2's bipartite cNLS in proteasomal nuclear localisation. In the canonical import pathway, cNLSs are recognised by importin-α (KPNA) proteins which form a heterodimer with importin-β1 (KPNB1)[2]. This aligns with our previous co-immunoprecipitation studies[8] that identified interactions of AKIRIN2 with KPNA2/3/4 and KPNB1, suggesting their involvement in this pathway. To test this hypothesis, we examined whether KPNA2/KPNB1 heterodimers recognize AKIRIN2's cNLS and facilitate proteasome recruitment. *In vitro* reconstitution using sucrose density gradients demonstrated that AKIRIN2 forms a complex with KPNA2/KPNB1 and mediates their association with the proteasome (Fig. 4a). This interaction depends on AKIRIN2's cNLS, as an AKIRIN2ΔNLS mutant failed to recruit KPNA2/KPNB1 despite retaining proteasome binding (Fig. 4a, Extended Data Fig. 7a). These results indicate that KPNA2/KPNB1 and IPO9 engage distinct binding sites on AKIRIN2, allowing non-competitive recruitment.

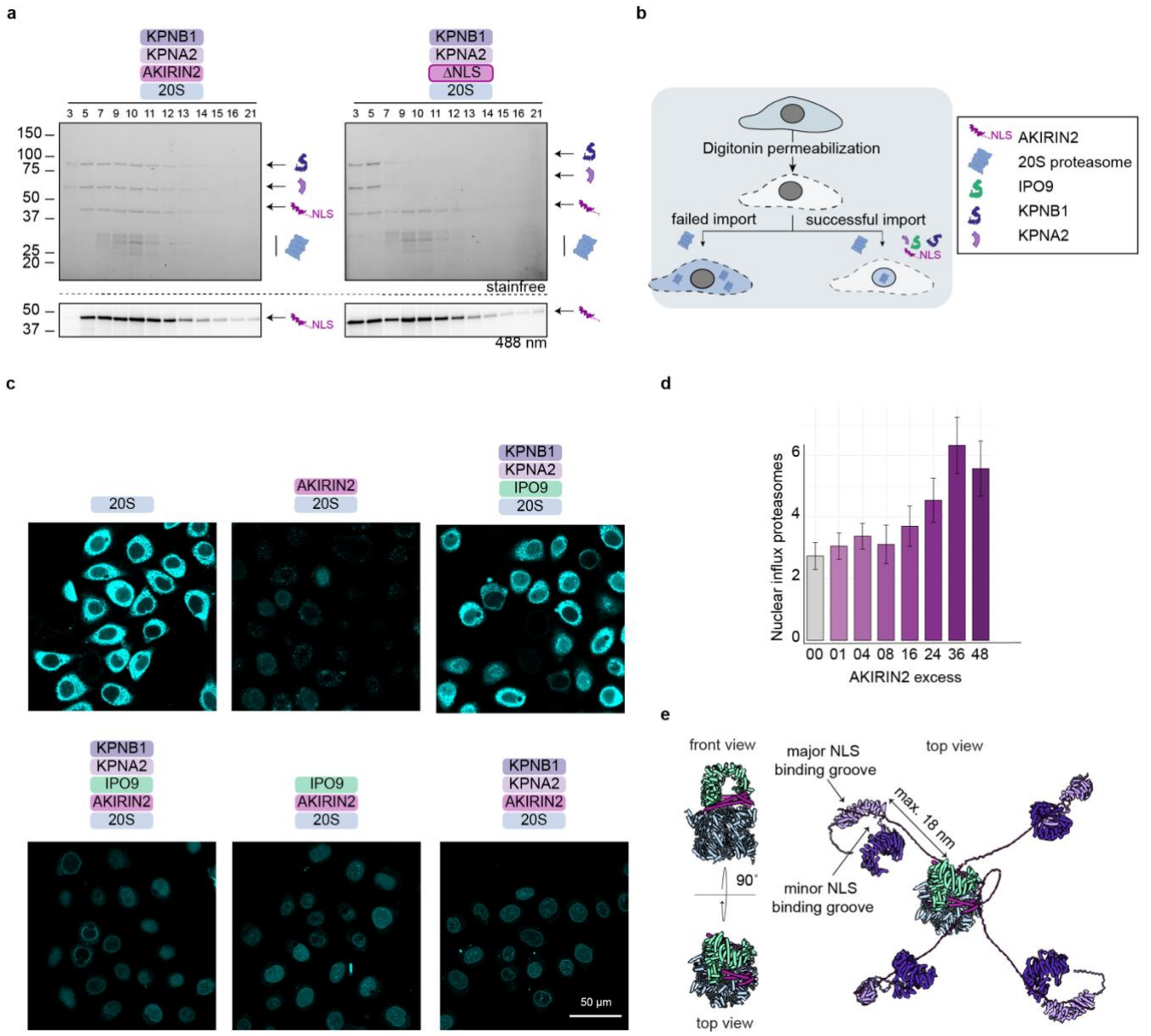

Fig. 4 | AKIRIN2 mediates formation of the canonical nuclear import machinery. **a**, Sucrose density gradients forming complexes with the proteasome and KPNA2/KPNB1 in the presence of AKIRIN2 (left) but not with the AKIRIN2ΔNLS mutant (right). **b**, Schematic of the nuclear import assay procedure. **c**, Representative confocal image of nuclear import of A647-20S labelled proteasome in digitonin permeabilized cells in different combinations of import factors. **d**, Quantified nuclear to cytoplasmic signal of A647-labelled proteasomes in nuclear import assays with increase of the AKIRIN2 concentration. **e**, Hybrid structural model, top view from the proteasome showing IPO9 (green) bound on top, each of the AKIRIN2 protomers (dark pink) can theoretically bind to an KPNA2/KPNB1 (purple) heterodimers.

We next assessed the sufficiency of these components for proteasome nuclear import using a minimal *in vitro* system (Fig. 4b). Proteasomes entered the nucleus only when both AKIRIN2 and importins (IPO9 and/or KPNA2/KPNB1) were present, with import efficiency increasing with AKIRIN2 concentration (Fig. 4c,d). Notably, either IPO9 or KPNA2/KPNB1 was sufficient for import in the presence of AKIRIN2, underscoring AKIRIN2's pivotal role.

While structural characterisation of the entire import complex proved challenging, likely due to the flexible nature of AKIRIN2 in its cNLS region, we generated a hybrid model combining our cryo-EM structure of the ternary complex with AF2 predictions of AKIRIN2:KPNA2:KPNB1 interactions (Fig. 4e, Extended Data Fig. 7b). This model suggests that each of the four AKIRIN2 protomers bound to IPO9 and the proteasome could independently associate with a KPNA2/KPNB1 heterodimer without steric hindrance (Fig. 4e). The flexibility of AKIRIN2's unresolved N-terminal region potentially allows importins to be positioned up to 18 nm from the proteasome surface, enabling simultaneous accommodation of at least five importin-β molecules (one IPO9 and four KPNA2/KPNB1 heterodimers) on one side of the 20S proteasome. Together, these findings reveal AKIRIN2 as a crucial adaptor that oligomerizes on the proteasome, with its extended, flexible structure providing the spatial arrangement necessary to engage multiple importin-β family members. This mechanism explains how proteasomes, incapable of directly binding importins, can efficiently traverse the nuclear pore complex.

Disassembly dynamics of the proteasome import complex

Efficient nuclear enrichment of imported proteins requires a disassembly mechanism upon nuclear entry[12], which is commonly mediated by RanGTP binding to importin-β family proteins[1]. To investigate whether the proteasome import complex follows this principle, we incorporated a dominant GTP-bound Ran mutant, Ran(1-180)Q69L[13], into our reconstitution experiments. The addition of RanGTP destabilized importin-proteasome complexes, resulting in a complete release of KPNA2/KPNB1. However, IPO9 and AKIRIN2 were only partially released from the 20S proteasome (Fig. 5a, Extended Data Fig. 3d), reminiscent of previously observed effects of RanGTPase on the H2A/H2B:IPO9 complex[10].

The incomplete dissociation of AKIRIN2 and IPO9 *in vitro* prompted us to investigate the release mechanism within the nucleus. Our previous work indicated that AKIRIN2 itself might be targeted for degradation by nuclear proteasomes[8], potentially providing an alternative pathway for import factor removal. To test this hypothesis, we treated RKO cells with either a proteasome inhibitor (MG132) or an E1 ubiquitin-activating enzyme inhibitor (TAK-243). MG132 treatment increased both AKIRIN2 and MYC levels compared to the DMSO control (Fig. 5b). E1 inhibition decreased overall ubiquitination and increased MYC levels but, surprisingly, did not prevent AKIRIN2 degradation, indicating that AKIRIN2 undergoes ubiquitin-independent proteasomal degradation, potentially facilitating the final release of proteasomes from their import machinery. Together, our findings suggest a two-step disassembly process for the proteasome import complex: an initial RanGTP-mediated release of canonical importins, followed by ubiquitin-independent degradation of AKIRIN2. This mechanism ensures complete liberation of imported proteasomes in the nucleus, allowing them to perform their critical functions in protein homeostasis and transcriptional regulation.

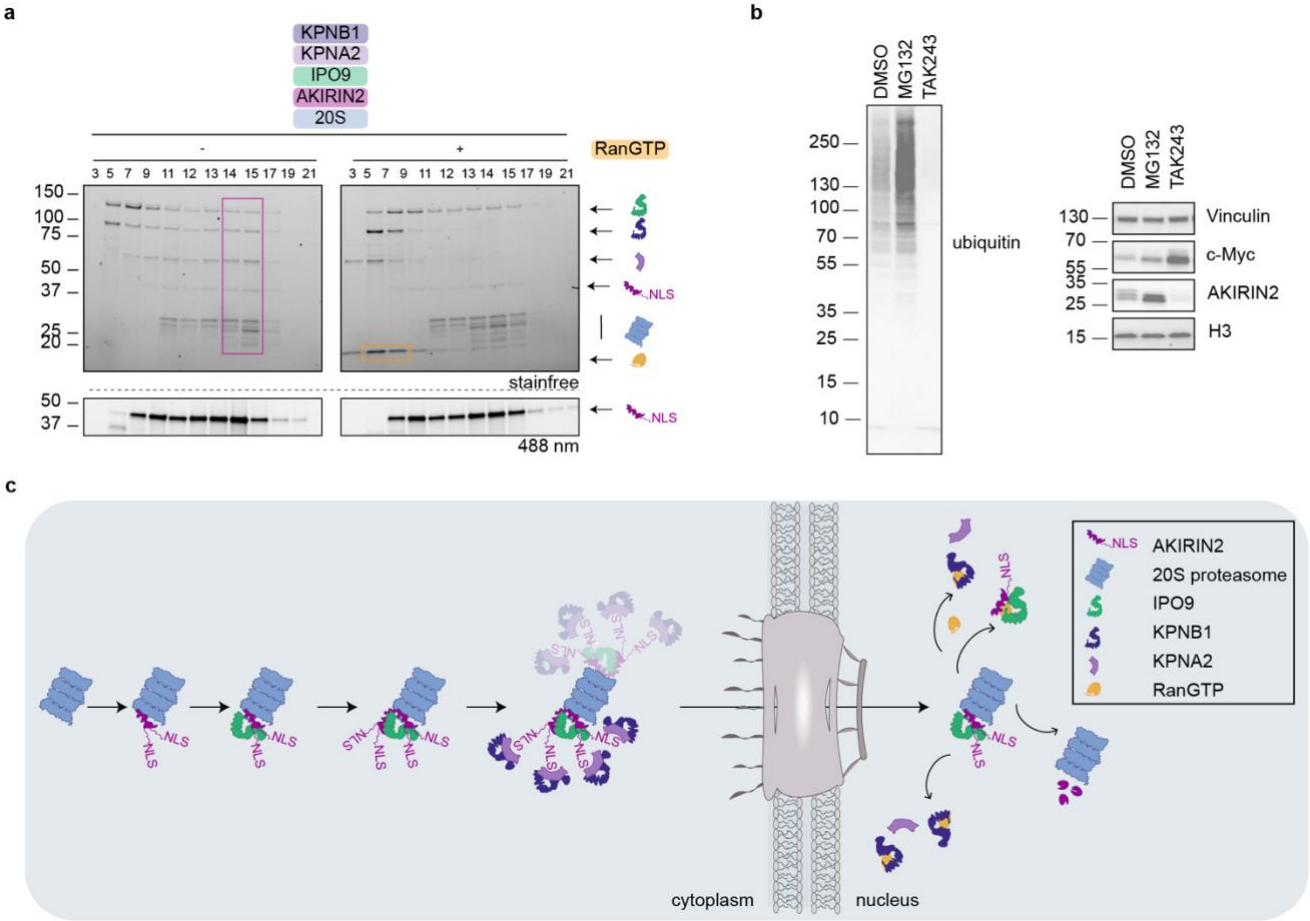

Fig. 5 | Dissociation of nuclear proteasome from the import machinery and ubiquitin-independent AKIRIN2 degradation. a, RanGTP addition disassembles complexes with KPNA2/KPNB1. **b**, Western blot of whole cell lysate of RKO cells treated with either proteasome inhibitor MG132, E1-inhibitor TAK243 or DMSO as control for 3 h against ubiquitin, AKIRIN2, MYC, vinculin, and H3. **c**, Schematic representation of suggested nuclear import pathway of the proteasome. Showing assembly and disassembly.

Discussion

Our study characterised the largely unstructured and multivalent import adaptor AKIRIN2. We reveal how AKIRIN2 recruits multiple importins to facilitate proteasome nuclear entry. Our structural and functional data elucidate a mechanism where AKIRIN2's conformational flexibility allows it to engage both the proteasome and importins, forming a transport-competent complex. AKIRIN2 binds to multiple sites on the proteasome and IPO9, leading to its oligomerization on the complex. This arrangement exposes AKIRIN2's N-terminal cNLSs, making them accessible to canonical import machinery. The resulting multimeric complex mobilizes numerous importins, enabling the large proteasome to traverse the nuclear pore complex. Upon nuclear entry, RanGTP dissociates most importins, while AKIRIN2 undergoes ubiquitin-independent proteasomal degradation, releasing the proteasome for its nuclear functions. The trigger for AKIRIN2 degradation post-import remains unclear, possibly the recently discovered midnolin-proteasome pathway[14], which targets nuclear proteins with similar characteristics, could be involved. Studies are currently missing which investigate into this direction.

This mechanism likely extends beyond proteasomes to other large protein complexes. Our findings, along with observations from viral capsid import studies, suggest that large cargos generally require multiple importins for nuclear entry[3,4,15]. While viral capsids like HBV achieve multi-importin recruitment through repetitive NLS display[15], our study reveals how endogenous complexes like proteasomes use adaptors like AKIRIN2 to similar effect.

Importantly, recent studies have identified proteins with analogous functions to AKIRIN2 for other proteins or complexes. These include Sts1/Cut8 for yeast proteasomes[16,17], HAPSTR1 for the giant E3 ligase HUWE1[18], VCF1/2 for the proteasomal

activator p97[19], and Fam172A for AGO2[20]. While these adaptor proteins lack sequence homology, they share a common architecture: a cargo-binding region, a long flexible linker, and an NLS for importin recruitment. This conserved structure suggests a universal mechanism for nuclear import of large complexes. These nuclear import adaptors serve three critical functions. First, they eliminate the need for cargos to display multiple NLSs, which could interfere with protein function. Second, they allow cells to modulate the localisation of large complexes without altering their expression levels, enabling rapid responses to cellular stress and other stimuli[21–23]. Lastly the oligomerization of nuclear import adaptors on cargo proteins may be a common strategy to present sufficient NLSs for efficient import, ensuring rapid nuclear translocation of essential complexes. This strategy allows cells to modulate the nuclear localisation of large complexes without altering their structure or compromising their function.

Our discovery of AKIRIN2's role in proteasome import unveils a previously unknown mechanism for nuclear import of large protein complexes. This finding has broad implications for understanding how cells rapidly adjust their nuclear proteome in response to various stimuli. Moreover, it opens new avenues for exploring the regulation of nuclear protein homeostasis and potentially developing therapeutic strategies targeting these processes in diseases involving aberrant protein degradation or nuclear function.

Methods

Cell culture

Human RKO (sex unspecified; American Type Culture Collection (ATCC) cat. no. CRL-2577, RRID:CVCL_0504) were cultured in RPMI 1640 (Gibco) supplemented with 10% FBS (Sigma-Aldrich), L-glutamine (4 mM, Gibco), sodium pyruvate (1 mM, Sigma-Aldrich) and penicillin/streptomycin (100 U/mL/, Sigma-Aldrich). Lenti-X lentiviral packaging cells (female, Clontech, cat. no. 632180) and HeLa cells (female; ATCC cat. no. CCL-2, RRID:CVCL_0030) were cultured in high-glucose Dulbecco's modified Eagle's medium (DMEM; in-house media kitchen) supplemented with 10% FBS, L-glutamine (2 mM, Gibco), sodium pyruvate (1 mM, Sigma-Aldrich) and penicillin/streptomycin (100 U/mL/, Sigma-Aldrich). All cell lines were maintained at 37 ºC with 5% CO2, routinely tested for mycoplasma contamination and authenticated by short tandem repeat analysis.

Lentivirus production and infections

Semiconfluent Lenti-X cells (Clontech, 632180) were co-transfected with lentiviral plasmids, pCMVR8.74 helper (Addgene plasmid no. 22036) and pCMV-Eco (Cell Biolabs) envelope plasmids using polyethylenimine (PEI) transfection (MW 25,000, Polysciences) as previously described[24]. The following day, media was replaced in the morning with target cell media and viral supernatant was harvested 48 and 72 h post transfection. Virus containing supernatant was clarified by centrifugation. Target cells were transduced by seeding them into a new 6well tissue culture dish and a few hours later addition of 0.5-1.5 mL virus supernatant.

Generation of a clonal iCas9 20S reporter cell line

RKO:iCas9-BFP cells [8] were lentiviral transduced with a lenti-pRRL.SFFV plasmid expressing human PSMB4 fused to StayGold (pcDNA3/er-(n2)oxStayGold(c4)v2.0 from Atsushi Miyawaki, RRID:Addgene_186296, construct was modified removing the ER-localisation signal) and a TwinStrep tag. Cells were then transiently transfected with lentiCRISPRv2-PSMB4_16-iRFP670 using transduction reagent Lipofectamin3000 and treated with 0.5 µg/mL of Doxycycline (DOX) (Sigma-Aldrich) to induce the knockout of endogenous PSMB4. Double-positive iRFP670/StayGold cells were sorted by flow cytometry, and further transduced with a lenti-SFFV-mCherry-MYC-IRES-BFP construct. Final reporter cells were isolated as single cells by flow cytometry, selecting for StayGold/BFP positives and iRFP negatives. The knockout of endogenous PSMB4 and the insertion of SFFV-mCherry-MYC-IRES-BFP was verified by PCR from genomic DNA and Sanger sequencing. The resulting clone was functionally tested for Cas9 induction/tightness by perturbation of essential genes +/- Dox, PSMB4-StayGold localisation by microscopy and mCherry-MYC induction by treatment with MG-132.

Generation and analysis of individual knockout or ectopic expression cell lines

The newly generated 20S reporter cell line was lentiviral transduced with either a dual-sgRNA (hU6-sgRNA-mU6-sgRNA-EF1αs-hCD2-Puro) targeting AKIRIN2-, KPNA2-, IPO9- or AAVS1, a single sgRNA (U6-sgRNA-mPGK-hCD2) targeting KPNB1 or PSMA3, or with a lentiviral plasmid containing an AKIRIN2 variant (pRRL-SFFV-AKIRIN2mutant-IRES-Thy1.1-Neo). Following transduction, cells were selected with antibiotics or FACS sorted by antibody staining of the co-expressed surface-markers (hCD2 and Thy1.1). For the knockout cells, Cas9 induction was induced by 0.2-0.5 µg/mL Doxycycline for 2-3 days. Cells were analysed by confocal microscopy. Therefore, they were seeded on ibidi 8well µ-slides the day before and imaged on a LSM 880 Axio Observer (inverted) with Airyscan /Airyscan fast with incubation chamber.

Construction of the human AKIRIN2 cDNA Mutagenesis Library

The construction of the AKIRIN2 cDNA mutagenesis library was organized into four sub-libraries, each covering approximately one-fourth of the AKIRIN2 coding sequence (50 amino acid residues). These sub-libraries together encompass every possible single amino acid substitution, including changes to any of the other 19 amino acids, deletions of individual residues, self-replacements (negative control), and mutations to STOP codons (positive control). A codon-optimized AKIRIN2 cDNA, modified to harbour point mutations at sgRNA cut sites, was engineered and tested for its ability to rescue endogenous AKIRIN2 knockout. For each sub-library, a different recipient vector was constructed, incorporating a specific landing site for oligonucleotide DNA inserts at the designated positions. Oligonucleotide pools encoding approximately 50 amino acids, flanked by Esp3I sites and specific primer binding sites, were synthesized by Twist Bioscience (~1200 oligos per pool). To ensure robust detection of mutants by next-generation sequencing (NGS), codons were altered to differ by at least two nucleotides from the template sequence wherever possible. The oligo pools were PCR amplified separately and cloned into the corresponding recipient vectors (pRRL-SFFV-PBSa-AKIRIN2mutant[Esp3I-filler-Esp3I]-PBSb-IRES-Thy1.1-Neo) using Esp3I Golden Gate assemblies with 48 cut-ligation cycles. The assembled constructs were purified and introduced into MegaX DH10B electrocompetent cells (ThermoFisher) by electroporation, followed by overnight culture and plasmid isolation after overnight culture. All four sub-libraries were cloned to achieve a representation exceeding 10,000 bacterial colonies per construct, verified by dilution series.

Saturation mutagenesis screen (SMScreen)

AKIRIN2 cDNA sub-libraries were transduced at a single-copy level into the 20S reporter cell line (RKO:iBFPCas9:PSMB4:StayGold:ΔPSMB4:mCherry-MYC-IRES-BFP) and selected using 500 µg/mL Neomycin. After confirming the selection of Thy1.1 positive cells, they were further transduced with an optimized dual-sgRNA construct targeting endogenous AKIRIN2 (dual-hU6-sgRNA1-mU6-sgRNA2s-hCD2-P2A-PuroR) and subsequently selected with 2 µg/mL Puromycin. The efficiency of each transduction step was assessed via FACS, analysing surface marker expression. Cells were cultured for up to four days and large batches, exceeding 10,000-fold library representation, were cryopreserved. To account for cell cycle variations, editing of endogenous AKIRIN2 was induced in a staggered manner (96 h, 72 h, and 48 h before the experiment) by adding 0.5 µg/mL Doxycycline. Each induction time point, and sub-library were maintained at representations above 10,000-fold.

Cell sorting involved two separate flow cytometry approaches: First, approximately 2-3% of cells displaying the highest mCherry levels were sorted by FACS. Second, cells were stained at a 1:25 ratio with DRAQ5 nuclear stain, and roughly 5% of cells at both the lowest and highest DRAQ5 correlations were sorted using an image-enabled cell sorter (ICS) from BD Biosciences. Sorted cells were centrifuged at 600 rcf for 5 min, and the cell pellets were immediately flash-frozen and stored at -80 °C until DNA isolation. Additional cells were collected 12 days post-Dox induction (dropout). Genomic DNA (gDNA) from dropout and t0 (uninduced) samples was isolated via phenol extraction, while gDNA from sorted samples was purified using NucleoSpin Blood Mini kits. All samples were amplified in nested PCR reactions using barcoded primers. The initial PCR amplified the region of interest within the AKIRIN2 cDNA over 27 cycles using one

primer flanking the cDNA and one intra-cDNA primer. DNA from all samples was then purified, quantified using Qubit Fluoro-DNA HS, and pooled at appropriate concentrations for a secondary PCR of 6 cycles to append sequencing adapters. Samples were sequenced on a NextSeq2000 P1 flowcell in Paired-end 300 read mode.

Saturation mutagenesis data analysis

The oligonucleotide insert libraries were indexed for Bowtie (v1.3.1) analysis (https://doi.org/10.1186/gb-2009-10-3-r25).
Initially, random 4-mer nucleotides were trimmed using Cutadapt (v4.8) (DOI:10.14806/ej.17.1.200) prior to the demultiplexing of reads by 8-mer sample barcodes, without allowing for mismatches. Following demultiplexing, additional trimming of barcodes and spacers was performed using Cutadapt, resulting in reads that exclusively covered the region of interest. These trimmed reads were then perfectly aligned using Bowtie with the parameters (--best --tryhard -v 0) and quantified using featureCounts (v1.6.1) (PMID: 24227677).
The raw counts were median-normalized, and fold changes between the sorted samples and reference points (either t0 or dropout) were calculated. The effects were scaled from 1 (representing strong enrichment, median from STOP controls) to 0 (indicating neutral effects, median from self-replacement controls), facilitating a more accurate cross-comparison of sub-libraries. To summarize the data effectively, a single score value was derived for each mutation, integrating individual comparison contrasts. The base for this integration was the scaled effects from the mCherry-MYC screen, which were then adjusted by a fraction derived from the PSMB4(α4) localisation screen results. Detailed analysis scripts are available upon request.

Validation of hits from the saturation mutagenesis screen

To validate individual hits from the saturation mutagenesis screen, cell lines expressing an AKIRIN2 variant were created using the methods described above– with DNA synthesized by Twist Biosciences. These cells were further transduced with the optimized dual-sgRNA targeting endogenous AKIRIN2 and selected using 500 µg/mL Neomycin and 2 µg/mL Puromycin. Transfection efficiency was evaluated by FACS, staining for the surface markers hCD2 and Thy1.1. Cells were analysed by confocal microscopy as described above. Additionally, cell lines with ectopic expression were assessed by FACS (Novocyte Penteon, Agilent), gating for mCherry-positive cells. Lysates from these cells were harvested after 3 days of DOX induction and analysed by Western blot, probing AKIRIN2 protein levels and using vinculin as a loading control.

Competitive profiling assay

To assess cell viability, cells were lentiviral transfected with sgRNA expression vector with 20-70% infection efficiency. sgRNA positive cells were sorted by flow cytometry staining the co-expressing surface or fluorescent marker. Cells were mixed with not transfected cells to a 70/30 (transfected/not-transfected) ratio. Knockout of the cells was induced for 1-8 days, cells were stained with an APC-conjugated anti-CD2 or anti-Thy1.1 antibody and the ratio of transfected cells was measured for each time point by flow cytometry.

20S purification

For expression and purification of 20S a slightly adapted protocol from[25] was used. The initial plasmids pACEBac1 containing α-subunits, pIDS vector containing β-subunits and pACEBac1 containing assembly chaperones PAC1-PAC2, PAC3-PAC4 and POMP were kindly provided by Prof. Fonseca. α-subunits from pACEBac1 vector and β-subunits from pIDS vector were combined on one pGBdest vector by Protech facility using golden gate. pGBdest vector containing all subunits and pACAEBac1 vector with all chaperones were transformed into DH10EmBacY chemically competent cells. Positive clones were selected using blue/white screening. The bacmids were purified using isopropanol precipitation and the recombination of the gene of interests were verified by PCR. The bacmids were transfected into Sf9 cells using polyethyleneimine (PEI) for the generation of the V0 stock, using YFP fluorescence as a measure of transfection efficiency. Following virus amplification in Sf9 suspension insect cell culture, constructs were expressed in Trichoplusia ni High-Five insect cells (Thermo Fisher) infected at a density of 1×10^6 cells/mL using 1:1 ratio of the 20S and the assembly chaperones viruses. Cells were grown at 100 rpm at 27 °C shaking using ESF921 serum-free growth medium (Expression Systems).

Cells were harvested 3 days after transfection by centrifugation at 2000 rcf for 20 min, and pellets were flash-frozen in liquid nitrogen and stored at –80 °C. The cell pellet was resuspended in 3x (w/v) of Buffer L1 (50 mM HEPES/NaOH pH 7.5, 500 mM NaCl, 1 mM EDTA, 0.5 mM TCEP) supplemented with Benzonase (IMP Molecular Biology Service). Cells were lysed using a glass Dounce homogenizer and subsequently centrifuged at 40,000 rcf for 1 h. The supernatant was applied on a pre-equilibrated StrepTrap HP column (Cytiva) equilibrated in Buffer L1. The column was washed with 10 column volumes (CV) of buffer P1 (50 mM HEPES/NaOH pH7.5, 150 mM NaCl, 1 mM TCEP) and eluted with Buffer P1 supplemented with 5 mM d-Desthiobiotin. The eluate was collected in fractions and desired fractions were combined, concentrated with a 100 kDa cut-off concentrator (Cytiva), and loaded on a Superose 6 16/70 column (Cytiva) equilibrated in buffer P1. For long-term storage, the desired fractions were combined, concentrated and flash-frozen in liquid nitrogen. Typical yield 5 mg from 1 L of Hi5 culture.

His-GFP-AKIRIN2/ His-GFP-AKIRIN2ΔNLS purification

His-GFP-AKIRIN2 was purified as previously described[26]. The mutant His-GFP-AKIRIN2ΔNLS (deletion of residues 8-28) was purified in the same way. Briefly, His-GFP-AKIRIN2 was expressed in BL21(DE3). Culture was inoculated into 6 L of autoinduction media supplemented with 50 µg/mL kanamycin and incubated at 37˚C for 5 h followed by 18˚C for 18 h. Cells were harvested at 2000 rcf for 20 min at 4˚C. The cell pellet was resuspended in buffer L2 (50 mM Tris-HCl pH 8, 500 mM NaCl, 0.5 mM TCEP) supplemented with 1x cOmplete protease inhibitor and Benzonase. The cell suspension was homogenized using French Press at 1.5 kbar and subsequently centrifuged at 40,000 rcf for 1 h at 4˚C. The supernatant was applied on a 5 mL HisTrap HP column (Cytiva) pre-equilibrated with buffer L2. Column was washed with 10 CV of 5% of buffer P2 (50 mM Tris-HCl pH8, 500 mM NaCl, 0.5 mM TCEP, 500 mM Imidazole pH8) and eluted with 50% of buffer P2. Fractions were pooled, concentrated with a 30 kDa cut-off concentrator (Cytiva) and loaded on a Superdex S200 16/60 column (Cytiva) equilibrated in buffer P3 (25 mM HEPES pH 7.5, 100 mM NaCl, 0.5 mM TCEP). Desired fractions were pooled, concentrated and flash-frozen in liquid nitrogen for long-term storage.

IPO9 purification

Srep-IPO9 (TS_pGC-01;02 from VBSF) was expressed in Arctic Express cells in autoinduction media supplemented with 20 µg/mL Gentamycin and culture was incubated for 37˚C for 5.5 h, followed by 16˚C for 24 h. Cells were pelleted 2000 rcf, 20 min. Pellet was flash frozen until further processing. Cells were resuspended in 250 mL buffer L3 (50 mM Tris 7.5, 300 mM NaCl, 0.5 mM TCEP) supplemented with 1x cOmplete protease inhibitor and Benzonase. The cell suspension was homogenized using French Press at 1.5 kbar and subsequently centrifuged at 40,000 rcf for 1 h. The supernatant was applied to a Strep Trap HP 5 mL which was before equilibrated with 5 CV buffer L3. Column was washed with 5 CV buffer L3 and eluted with 5 CV 3 mL/min buffer P4 (buffer L3 + 5 mM d-Desthiobiotin). Desired fractions were pooled and applied on a ResQ (6 mL) column which was equilibrated with buffer P5 (50 mM Tris 7.5, 50 mM NaCl, 0.5 mM TCEP). After sample application column was washed with 5 CV buffer P5 and then eluted with 20 CV up to 37% gradient increasing concentration of buffer P6 (50 mM Tris pH7.5, 2 M NaCl, 0.5 mM TCEP). Desired fractions were pooled and loaded on a Gel Filtration (Hiload 16/600 Superdex 200) column which was equilibrated with buffer P7 (40 mM Tris 7.5, 50 mM NaCl, 0.5 mM TCEP). Sample was eluted with 1 CV of buffer P7. Desired fractions were pooled and concentrated in 30 kDa cutoff 15 mL tubes.

KPNB1 purification

Human KPNB1 was cloned into pQE-60 and expressed in E. coli SG13009 cells grown in 2YT to an OD600 = 0,6-0,8 at 37 °C and afterwards induced with 0.5 mM IPTG (additional 30 mM K2HPO4 added for buffering). Cultures were incubated at 18 °C overnight and harvested by centrifugation 5749 rcf for 30 min at 4˚C. The pellet was dissolved in 30 mL 1x PBS (2.7 mM KCl, 140 mM NaCl, 8.6 mM Na_2HPO_4, 1.5 mM KH_2PO_4 pH 7.4). Cells were centrifuged at 4147 rcf for 15 min at 4˚C and the pellet was flash frozen in liquid nitrogen and stored at -20˚C until further use. For purification the pellet was solved in buffer L4 (50mM Tris/HCl pH 7,5, 150 mM NaCl, 10 mM KCl, 1 mM $MgCl_2$,

10 mM Imidazole) and lysed with a high-pressure homogenizer (Microfluidics) with 15000 psi, at 4˚C. Lysate was centrifuged at 30000 rcf for 30 min at 4˚C. The supernatant was applied to a His-Trap column (10 mL final volume, either from Macherey Nagel or Cytiva). Column was washed with buffer L4+70 mM Imidazole to remove unspecific bound proteins and afterwards KPNB1 was eluted by increasing the Imidazole concentration to 250 mM. Desired fractions were analysed by SDS-PAGE and the respective fractions pooled and concentrated to 3.5-4 mL before loading on a size exclusion chromatography (Superdex 200 26/60 or 16/60), which was equilibrated in buffer P8 (20 mM Tris/HCl pH 7,5, 150 mM NaCl, 2 mM $MgCl_2$). Eluted peak fractions were analysed by SDS Page. Desired fractions were combined and concentrated in 50 kDa cutoff concentrators to a concentration of >10 mg, flash frozen and stored at -80˚C.

KPNA2 purification

Human KPNA2 cDNA was cloned into His vector pRSET (Invitrogen) using BamHI and XhoI restriction sites[27]. For expression of KPNA2 was transformed into the E. coli strain BL21 (DE3) LysS and the cells were grown to OD600 of 0.6 and induced with 0,5 mM IPTG for 4 h at 30 °C. Cells were harvested by centrifugation 5749 rcf for 30 min at 4˚C. The pellet was dissolved in 30 mL 1x PBS (2.7 mM KCl, 140 mM NaCl, 8.6 mM Na_2HPO_4, 1.5 mM KH_2PO_4 pH 7.4). Cells were centrifuged at 4147 rcf for 15 min at 4˚C and the pellet was flash frozen in liquid nitrogen and stored at -20˚C until further use. Cells from a 3 L culture were lyzed in buffer L5 (50 mM Tris pH 7.5, 500 mM NaCl) with a French Press and recombinant KPNA2 was purified twice over Ni-nitrilotriacetic acid agarose (Qiagen) under native conditions step wise eluting with buffer P9 (50 mM Tris pH 7.5, 500 mM NaCl, 20, 60 and 300 mM Imidazole). Respective elution fractions were combined and concentrated to 3.5-4 mL and loaded on a size exclusion chromatography (Superdex 200 26/60 or 16/60) which was equilibrated in buffer P8 (20 mM Tris/HCl pH 7,5, 150 mM NaCl, 2mM $MgCl_2$). Proteins were eluted with 1 CV buffer. Desired fractions were combined and concentrated in 30 kDa cutoff concentrators to a concentration of >1 mg, flash frozen in liquid nitrogen and stored at -80˚C.

His-GST-mCherry purification

mCherry construct was cloned into a pETM33 plasmid and was expressed in BL21(DE). Culture was inoculated into 4 L of autoinduction media supplemented with 50 µg/mL Kanamycin. Culture was growing at 37˚C for 5.5 h, followed by 16˚C for 24 h. Culture was spun down at 2000 rcf for 30 min. Pellet was resuspended in 150 mL lysis buffer L3 supplemented with 1x cOmplete protease inhibitor and Benzonase. The cell suspension was homogenized using a French Press at 1.5 kbar and subsequently centrifuged at 40,000 rcf for 1 h at 4˚C. Supernatant was loaded on two HisTrap columns (5 mL each) in a row which were before equilibrated with 2 CV ddH2O, and 5 CV buffer L3. Columns were washed with 20 CV wash of 5% buffer P10 (50 mM Tris 7.5, 0.5 M Imidazole, 300 mM NaCl, 0.5 mM TCEP) and afterwards eluted with 10 CV 50% buffer P10, followed by 5 CV 100% buffer P10. Desired fractions were combined and loaded on a GST Trap crude column 5 mL which was equilibrated with buffer P11 (50 mM Tris pH8, 0.3 M NaCl, 0.5 mM TCEP). Column was washed with 20 CV buffer P11 and eluted with 5 CV buffer P11 supplemented with 15 mM GSH and re-adjusted pH to 8. Desired fractions were combined and dialyzed overnight in 1 L buffer P12 (50 mM Tris 7.5, 150 mM NaCl, 0.5 mM TCEP) and concentrated in a 6 mL 10 kDa cutoff concentrator at 4000 rcf for 30 min at 4˚C to a concentration of 12 mg/mL.

Ran purification

Human His_{10}-tagged Ran (residues 1:180) was cloned into a (pETM14 plasmid) was expressed in Rosetta2 cells. Culture was inoculated into 4 L of autoinduction media supplemented with 50 µg/mL Kanamycin. Culture was spun down at 2000 rcf for 30 min at 4˚C. Pellet was resuspended in 200 mL buffer L6 (20 mM Tris pH8.0, 0.5 M NaCl, 0.5 mM TCEP) supplemented with 1x cOmplete protease inhibitor and Benzonase. The cell suspension was homogenized using French Press at 1.5 kbar and subsequently centrifuged at 40,000 rcf for 1 h at 4˚C. Supernatant was loaded on a His Trap column 5 mL which was equilibrated with buffer L6. After sample application column was washed with 5% buffer P13 (20 mM Tris pH8.0, 0.5 M Imidazol, 0.5 M NaCl, 0.5 mM TCEP) and eluted with 10 CV 50% and 5 CV 100% buffer P13. Desired fractions were combined and diluted with buffer P14 (50 mM

Tris 8.0, 50 mM NaCl, 0.5 mM TCEP) to a salt concentration of about 50 mM NaCl and loaded on a ResQ column which was equilibrated with buffer P14. Elution with 20 CV up to 37% gradient increasing concentration of buffer P15 (50 mM Tris, 2 M NaCl, 0.5 mM TCEP). Sample was afterwards applied to a S200 size exclusion column which was equilibrated with buffer P16 (20 mM HEPES 7.5, 100 mM NaCl, 0.5 mM TCEP). Desired fractions were combined and concentrated with a 10 kDa cutoff concentrator to either 1 or 1.6 mg/mL.

RanGTP purification

Human His_{10}-tagged RanGTP Q69L (residues 1-180) was expressed in Rosetta (DE3) pLys, 4 L TB with Kanamycin and Chloramphenicol, induced at OD600 ~1, grown overnight at 18˚C. Resuspended in buffer P17 (50 mM K-Phosphate pH 7.0, 500 mM NaCl, 5 mM $Mg(OAc)_2$, 1 mM EDTA, 10 mM imidazole and 2 mM DTT) supplemented with 100 mM PMSF, 1x cOmplete protease inhibitor, 10 mg/mL DNAse I and 1 mg/mL lysozyme, and lysed by sonication (3:30, 70%, 0.5/0.5). 20 µM GTP was included in all purification buffers. Purification was done as previously described[28].

Antibodies

The following antibodies were used for western blot analysis: AKIRIN2 (HPA064239, Atlas Antibodies, RRID:AB_2685222, 1:1,000), c-MYC (D84C12, no. 5605, Cell Signaling Technology, RRID:AB_1903938, 1:1,000), HRP-anti-Histone H3 (3H1, Cell Signaling (1:1,000), IPO9 (PA5-25477, Invitrogen, rabbit, polyclonal antibody, RRID:AB_2542977) (1:1,000), Anti-vinculin ms (1:400) (V9131, Sigma, RRID:AB_477629).

Secondary antibodies: HRP anti-rabbit IgG (7074, Cell Signaling Technology, RRID:AB_2099233, 1:10,000), HRP anti-mouse IgG (7076, Cell Signaling Technology, RRID:AB_330924, 1:10,00).

Antibodies used for FACS analysis: APC anti-CD90.1/Thy1.1 (202526, BioLegend, RRID: AB_1595470, 1:500), APC anti-Hu/NHP hCD2 (17-0029-42, Invitrogen, RRID:AB_10805740, 1:500).

Immunoprecipitation

For Co-immunoprecipitations assays 1 nmol bait protein which is either Strep-IPO9 or as a control uncharacterised zinc finger protein 1 (organism: leptonema illini) as a control was added each in triplicates to 6.5 mL HeLa lysate which was supplemented with 4 mM ATP, 1 mM DTT (both to keep proteasomes stable), 0.1 mM PMSF, 2 mg/mL BSA. Per trial 50 µL slurry of Strep-Tactin high performance Sepharose (Cytiva 28-9356-00) was used and washed twice with work buffer (25 mM Bis Tris pH 6.5, 50 mM KCl, 5 mM $MgCl_2$, 4 mM ATP, 1 mM DTT) and to block unspecific binding beads were incubated for 30 min, rotating on RT with work buffer supplemented with 2 mg/mL BSA. Afterwards beads were added to the lysate and incubated for 2 h, 4˚C, rotating. Afterwards beads were spun down 500 rcf, 5 min, 4˚C. Aliquots from the supernatant were taken for analysis and rest was discarded. Beads were washed 6x with 1 mL work buffer. Proteins were eluted two times by adding 200 µL elution buffer (work buffer + 5 mM d-Desthiobiotin), incubating for 30 min, 4˚C, rotating. Beads were centrifuged 500 rcf, 1 min and supernatant was transferred. Samples were analysed on SDS-PAGE. Remaining samples was acetone precipitated (add 4x access of ice cold (-20˚C) Acetone to a final concentration of 80% to the samples, vortex and incubate at -20˚C, overnight, pelleted for 10 min at 10,000 rcf at 4 °C, dissolve pellet in 50 µL 20 mM Tris pH 7.5, 50 mM NaCl), and submitted for mass spectrometry analysis.

Mass spectrometry analysis

Samples were supplemented with 10 mM Dithiothreitol (DTT) and were heated to 95 °C for 10 min. Iodoacetamide (IAA) was added to a final concentration of 20 mM and the samples were incubated for 30 min at room temperature in the dark. The reaction was quenched by addition of DTT to 5 mM and incubated again 30 min at room temperature. 400 ng trypsin (Promega, Trypsin Gold) were added followed by an overnight incubation at 37 °C. The samples were acidified with trifluoroacetic acid (TFA, Pierce) to a final concentration of 1%. The nano HPLC system (UltiMate 3000 RSLC nano system) was coupled to an Orbitrap Exploris 480 mass spectrometer equipped with a Nanospray Flex ion source (all parts Thermo Fisher Scientific). Peptides were loaded onto a trap column (PepMap Acclaim C18, 5 mm × 300 µm ID, 5 µm particles, 100 Å pore size, Thermo Fisher Scientific) at a flow rate of 25 µL/min using 0.1% TFA as mobile phase. After loading, the trap column was switched in line with the analytical

column (PepMap Acclaim C18, 500 mm × 75 µm ID, 2 µm, 100 Å, Thermo Fisher Scientific). Peptides were eluted using a flow rate of 230 nL/min, starting with the mobile phases 98% A (0.1% formic acid in water) and 2% B (80% acetonitrile, 0.1% formic acid) and linearly increasing to 35% B over the next 120 min. This was followed by a steep gradient to 95%B in 5 min, stayed there for 5 min and ramped down in 2 min to the starting conditions of 98% A and 2% B for equilibration at 30 °C.The Orbitrap Exploris 480 mass spectrometer was operated in data-dependent mode, performing a full scan (m/z range 350-1200, resolution 60,000, normalized AGC target 300%, minimum intensity set to 10,000 and compensation voltages CV of -45 V and -60 V), followed by MS/MS scans of the most abundant ions for a cycle time of 1.0 second per CV. MS/MS spectra were acquired using an isolation width of 1.0 m/z, normalized AGC target 200%, HCD collision energy of 28 and orbitrap resolution of 45,000. Precursor ions selected for fragmentation (include charge state 2-6) were excluded for 45 s. The monoisotopic precursor selection (MIPS) mode was set to Peptide and the exclude isotopes feature was enabled. Data processing protocol: For peptide identification, the RAW-files were loaded into Proteome Discoverer (version 2.5.0.400, Thermo Scientific). All MS/MS spectra were searched using MSAmanda v2.0.0.16129[29]. The peptide mass tolerance was set to ±10 ppm and fragment mass tolerance to ±8 ppm, the maximum number of missed cleavages was set to 2, using tryptic enzymatic specificity without proline restriction. Peptide and protein identification was performed in two steps. For an initial search the RAW-files were searched against the human reference database (20,541 sequences; 11,3957,48 residues), supplemented with common contaminants and sequences of tagged proteins of interest using Iodoacetamide derivative on cysteine as a fixed modification. The result was filtered to 1 % FDR on protein level using the Percolator algorithm[30] integrated in Proteome Discoverer. A sub-database of proteins identified in this search was generated for further processing. For the second search, the RAW-files were searched against the created sub-database using the same settings as above and considering the following additional variable modifications: oxidation on methionine, glutamine to pyro-glutamate conversion at peptide N-terminal glutamine and acetylation on protein N-terminus. The localisation of the post-translational modification sites within the peptides was performed with the tool ptmRS, based on the tool phosphoRS[31]. Identifications were filtered again to 1% FDR on protein and PSM level, additionally an Amanda score cut-off of at least 150 was applied. Proteins were filtered to be identified by a minimum of 2 PSMs in at least 1 sample. Protein areas have been computed in IMP-apQuant[32] by summing up unique and razor peptides. Resulting protein areas were normalised using iBAQ[33] and sum normalisation was applied for normalisation between samples.

Sucrose density gradients

Density gradient centrifugations were performed by preparing the low-density solution of 10% (w/v) sucrose and high-density solution of 30% (w/v) sucrose in reconstitution buffer (20 mM phosphate buffer pH7.5, 50 mM NaCl, 4 mM ATP, 1 mM DTT). Gradients were made by mixing the two solutions using the Gradient Master (Biocomp systems) to create a continuous sucrose gradient. All compared gradients were performed in parallel using the same input protein concentrations (if not mentioned otherwise 40 pmol 20S proteasomes, 400 pmol of AKIRIN2 and 200 pmol of IPO9, KPNA2, KPNB1). The sample was prepared in 200 µL reconstitution buffer and applied on top of the density gradient prepared in an open-top 4.2 mL ultracentrifuge tube and run for 16 h at 165,000 rcf in an SW60Ti rotor. Gradients were manually fractionated into 200 µL fractions and analysed with stain-free and fluorescence imaging using Chemi-DocMP System (BioRad). For western blot analysis, up to 20 µL samples were usually applied to 4-20% TGX Stain-Free™ Protein Gel (BioRad), and run at 200 V for 45 min. Gel was transferred to a nitrocellulose membrane and probed for the desired proteins (e.g. AKIRIN2, IPO9).

Proteasome labelling with A647

To label 20S proteasomes with Alexa-647, recombinantly expressed 20S proteasomes with a concentration of 3 g/L were adjusted to a pH8 by adding 1.5 M HEPES pH8.3. Alexa-647-NHS dye was added to a final concentration of 100 µM. Reaction was incubated at 4˚C overnight (18 h). Reaction was quenched with 100 mM Tris pH 7.5. labelled 20S proteasomes were separated from free

remaining dye with size exclusion chromatography S6 increase 10/300 GL. Column was equilibrated with 20 mM HEPES pH7.3, 150 mM NaCl, 0.5 mM TCEP. Sample is applied over a 1 mL loop which is emptied with 2 mL of the buffer and then eluted with 1 CV, fractionated into 500 µL fractions. Desired fractions are analysed by SDS-PAGE and combined.

Cryo-EM sample preparation

For cryoEM analysis, complexes were reconstituted by sucrose density gradients, desired fractions were buffer exchanged in the reconstitution buffer excluding the sucrose using zeba spin desalting columns or 30/100 kDa cutoff concentrators (ThermoFisher). Grids were glow-discharged with BalTec SCD 005 sputter coater for 60 s at 25 mA using residual air. For the 20S:AKIRIN2:IPO9 sample R3.5/1 200 mesh Cu prefloated with 2 nm Carbon (Quantifoil) were used for plunge freezing. For the IPO9:AKIRIN2 sample open-hole R1.2/1.3 grids (Quantifoil) with 200 mesh. 4 µL of the sample was applied onto the treated side, and subsequently incubated for 2 s and front-side blotted using the Leica GP2 plunge freezer. Initial grid screening was performed on the 200 kV Glacios microscope (ThermoFisher) using the Falcon III detector (Thermo-Fisher). For the high-resolution 20S:AKIRIN2:IPO9 structure determination, data collection was performed on a 300 kV Titan Krios G2; Bio Quantum K3 equipped with a cold field emission gun and a post-column Selectris energy filter (ThermoFisher) with a 20 eV slit width and a Falcon 4 or Falcon 4i direct electron detector (ThermoFisher). Images were collected at a pixel size of 1.06 Å/pix with a cumulative dose of 44.4 e/Å^2 in eer format using a defocus range in -1.0 to -1.9 µm in 0.2 µm increments. For the high-resolution AKIRIN2:IPO9 structure determination data collection was performed on a 300 kV Titan Krios G4 equipped with a cold field emission gun and a post-column Selectris energy filter (ThermoFisher) with a 10 eV slit width and a Falcon 4 or Falcon 4i direct electron detector (ThermoFisher). Images were collected at a pixel size of 0.951 Å/pix with a cumulative dose of 40 e/Å^2 in eer format using a defocus range in -1.0 to -2.0 µm in 0.25 µm increments.

Cryo-EM image processing

The 9,366 movies of the 20S:AKIRIN2:IPO9 datasets were patch motion corrected and patch CTF estimated in cryoSPARC (v 3.2)[34]. 2D templates were generated by manually picking ~770 particles followed by 2D classification. Selected averages were used to for template picking and particles were extracted (boxsize 300 px, 1.07 Å/px). Particles were sorted by performing three rounds of 2D classification with particles separated into 6 equally sized batches. Next, ab-initio reconstruction and heterogeneous refinement were used to exclude badly resolving particles and 20S particles bound by proteasomal chaperones as previously reported[35]. Particles were reextracted (400 px, 1.07 Å/px) and refined via non-uniform refinement imposing a C2 symmetry after one further round of 2D classification (cryoSPARC v 4.2.1). Resulting poses were used for C2 symmetry expansion and signal of one half of the particles was subtracted along the symmetry axis. Following ab-inito reconstruction and heterogenous refinement, particles were downsampled (200 px boxsize, 2.14 Å/px), converted into star files using cs2star/pyem (https://github.com/brisvag/cs2star,)[36] and refined in relion (v 5.0)[37]. Next, two rounds of 3D classification without image alignment (Regularization parameter T=40) and blush regularisation[38] were performed. A map with a well-defined IPO9 density was used as a reference for an heterogenous refinement in cryoSPARC sorting particles which were initially imported into relion. IPO9 bound particles were then again imported into relion and 3D classified with image alignment (T=4) further excluding badly resolving particles. Next, particles were reextracted (300 px boxsize, 1.43 Å/px) once refined without a mask followed by a focussed refinement with a mask encompassing the AKIRIN2 and IPO9 denisty. To reduce conformational heterogeneity, particles were 3D classified without image alignment (T=100). The better resolving class was refined in cryoSPARC or in relion before performing local refinements on the 20S alpha-ring and the IPO9: AKIRIN2 densities or the densities of IPO9 and the second AKIRIN2 dimer, respectively. Local resolution was estimated for both refinements in cryoSPARC. The final maps were post-processed using DeepEMhancer[39] using the developer provided 'highRes' weights. The pixelsize was corrected to 1.055 px/Å (1.407 in the final map). The composite map was generated using

the 'volume zone' command in chimeraX to exclude regions of either the consensus or local refinement. Due to these manipulations this artificial 'frankenmap' was only used for visualisation purposes. The movies of the apo-IPO9:AKIRIN2 dataset were patch motion corrected and patch CTF estimated in cryoSPARC live (v 4.1.1) and micrographs were curated based on defocus and CTF-fit values resulting in 7,734 exposures. Particles were picked using cryolo (v 1.9)[40] by refining the pretrained weights, provided by the developers, using 10 manually picked micrographs. Particles were randomly split into 6 separate batches and sorted in three rounds of 2D classification using optimized parameters. Particles were sorted by performing ab-initio reconstruction and using the resulting maps as reference for a heterogeneous refinement. To increase the number of particles, the final coordinates of 20 micrographs were used to further refine the cryolo weights and pick the whole dataset. These particles were sorted by iteratively performing ab-inito reconstructions and using noisy and dirt maps as decoys to exclude respective particles in heterogenous refinements. The cleaned particle stacks of both cryolo trainings were combined, duplicates removed and reextracted (120 px boxsize, 1.59 Å/px), imported into relion and particles were refined using blush regularization. GSFC and local resolution was estimated in cryoSPARC using the relion half-maps. The 3D refined map was postprocessed using DeepEMhancer.

Cryo-EM model refinement

As an initial model for the 20S:AKIRIN2:IPO9 PDB-7NHT was used, together with AlphaFold2 predictions[41] for IPO9 and the AKIRIN2:dimers. . Proteasomal subunits, the AKIRIN2:dimer I, AKIRIN2:dimer II wing helix and IPO9 residues 696-1041 were modelled in the consensus 3D refined map. The AKIRIN2:dimer II and IPO9 residues 1-695 were modelled in the local refined map. Structures were fitted into the cryoEM maps via rigid body fitting in chimeraX (v.18)[42,43] and unresolved regions of AKIRIN2 and IPO9 were removed and structures fitted into cryoEM maps by flexible fitting using the namdinator web interface (https://namdinator.au.dk/)[44]. Structures were manually built by iteratively using Isolde (v 1.8[43,45,46]) and/or Coot (v 0.9.8[47–49]) followed by real space refinement in Phenix (v 1.21[49–52]). The composite model was generated by combining models from the consensus and local refinements, generating a covalent bond between IPO9 residues 695 & 696 and refining the bond's geometry in Isolde. The initial models for the IPO9 and the AKIRIN2 dimer were generated using AlphaFold2, unresolved regions were removed and structure fitted into the cryoEM maps using flexible fitting using the namdinator web interface (https://namdinator.au.dk/)[44]. The model was refined using Rosetta via iterative local rebuilding. The protocol was run 1000 times. The 25 best models according to the resulting energies where manual inspected[53].

Nuclear import assays

For the nuclear import assays, Hela cells were seeded 1-2 days before the experiment on ibidi 8well µ-slides in 300 µL DMEM to reach a cell density of 70-80% the day of the experiment.

On the day of the experiment the dish was placed on ice and cells were washed once with PBS and twice with freshly prepared transport buffer (20 mM HEPES pH7.3, 110 mM KOAc, 2 mM $Mg(OAc)_2$, 1 mM EGTA, 2 mM DTT, 1 mM PMSF, 1x cOmplete protease inhibitor). For permeabilization of the cellular membrane cells were incubated with 0.005% digitonin in transport buffer for 5 min on ice. Afterwards, cells are thoroughly but carefully washed 3x with transport buffer (2x3 min, 1x15 min). In the meantime, import mixes are prepared in transport buffer supplemented with an ATP regeneration mix (1 mM ATP, 10 mM PEP, 20 U/mL phosphokinase), 2 mg/mL BSA, 4 µM Ran, 2 µM mCherry (exclusion marker). In the different trials combinations of A647-labelled 20S proteasomes, GFP-AKIRIN2, IPO9, KPNA2 and KPNB1 are added. Import mixes are added to the permeabilized cells and the dish is incubated for 30-60 min at 30˚C in a humidity chamber. Cells are washed 2x with transport buffer and once with PBS. Cells are incubated with 0.1 µg/mL HOECHST 33342 in PBS for 10 min in the dark on RT. Cells are washed once more with PBS and imaged in PBS immediately after on an Olympus IX83 Spinning Disk Confocal SoRa equipped with a Yokogawa W1 spinning disk microscope.

NIA quantification

To determine fluorescent intensities a custom Fiji[54] macro was created. Cellpose 2.0[55] was used to

segment nuclei and cytoplasm and define ROIs for the measurements. Therefor we modified two pretrained models, retraining them with our own data and annotations, using Dapi for nuclear segmentation and Ch2 for defining the cytoplasm. Within the macro we ran Cellpose using our models on each image, then combining the resulting ROIs and measuring mean intensities in all channels.

MST binding affinity measurement

For the sample preparation GFP-labelled AKIRIN2 and IPO9 were prepared in BufferMST (50 mM Tris pH7.5, 150 mM NaCl, 0.005% Tween-20). Samples were spin filtered (Ultrafree-MC-HV Durapore PVDF 0.45 µm Centrifugal Filters) after which concentrations were determined at 488 nm for GFP-AKIRIN2 and at 280 nm (corrected for scattering at 333 nm) for IPO9 in a 0.15 cm cuvette using the according extinction coefficients. For the MST measurement different dilutions of GFP-AKIRIN2 were tested for its signal in the NT.115 Monolith in different capillary types at different MST powers. A final concentration of 13 nM for GFP-AKIRIN2, premium capillaries and medium MST power were concluded to be used for the binding experiments. Three replicates of a 15 point 1:1 dilution series of IPO9 with 14.1 µM as highest concentration and a 16th point without IPO9 were measured. The interaction was measured once without additives and once with 7.7 µM Ran and 1 mM GTP present in all samples. Samples have been incubated for about 10 min at RT prior to the measurement. For the data analysis hot and cold regions were selected from ~[-1 s, 0 s] and [1 s, 5 s] IR-Laser on-time respectively (Extended Data Fig. 3e). Data has been analysed and exported from MO. Affinity Analysis for replotting. PALMIST was used to quantify the equilibrium dissociation constants (K_{DS}) of the binding curves. The best fit K_{DS} as well as the non-symmetric 95% confidence intervals were returned.

Grating-coupled interferometry

The Creoptix WAVE system (Malvern Panalytical) was used to perform 20S Proteasome-AKIRIN2 binding experiments. All experiments were performed on 4PCP WAVEchip (Malvern Panalytical). The chip was first conditioned with 100 mM sodium borate pH9 and 1 M NaCl, followed by immobilization of 2000 pg/mm^2 20S proteasome on the measurement channel and BSA on measurement and reference channel using standard amine-coupling (activation with 1:1 mix of EDC/NHS, binding of 20S proteasome and BSA with sodium acetate pH4, quenching with 1 M ethanolamine pH8). 0.1X PBS was used as running buffer during immobilization. BufferGCI (50 mM TRIS pH7.5, 100 mM NaCl, 0.005% Tween-20, 1 mg/mL BSA, 1 mM TCEP) was used during the experiment. AKIRIN2 was injected in a 1:1 dilution series in the range of 93.75 nM – 12 µM in BufferGCI at 25 °C. Measurements were performed in three replicates, with a regeneration step between each set of replicates using BufferGCI supplemented with NaCl to reach 300 mM. Data was double referenced using a reference channel subtracted from the measurement channel and blank injections. Individual injections were bulk corrected, correction and analysis were performed using the Creoptix WAVEcontrol software (Malvern Panalytical). A one-to-one binding model was applied to fit the experiment.

E1 and proteasome inhibition

The day before the actual experiment, RKO cells were seeded on 3x10 cm tissue culture dishes. The next day cell density was about 60-70% and cells were either treated with 10 µM MG132 (proteasome inhibitor), 0.75 µM TAK-243 (E1-inhibitor) or 5 µL DMSO (control) each for 4 h. Afterwards cells were harvested with a cell scraper, washed once with PBS and lysed in RIPA buffer (50 mM Tris pH8, 150 mM NaCl, 1% Triton, 0.5% sodium deoxycholate, 0.1% SDS) supplemented with 1x cOmplete protease inhibitor, incubated for 20 min on ice, spun down full speed 21,300 rcf, for 10 min. Supernatant was transferred into a fresh tube and concentration was measured with Bradford. From each sample aliquots containing 35 µg total protein were taken and SDS loading dye was added. Samples were cooked for 5 min, cooled down, and loaded on a 4-20% TGX Stain-Free™ Protein Gel (BioRad) and run at 200 V for 45 min. Gel was transferred to a nitrocellulose membrane and probed for the desired proteins (AKIRIN2, c-MYC, ubiquitin, vinculin and histone H3).

References

1. Görlich, D. & Kutay, U. Transport Between the Cell Nucleus and the Cytoplasm. *Annu. Rev. Cell Dev. Biol.* **15**, 607–660 (11/1999).
2. Wing, C. E., Fung, H. Y. J. & Chook, Y. M. Karyopherin-mediated nucleocytoplasmic transport. *Nat. Rev. Mol. Cell Biol.* (2022) doi:10.1038/s41580-021-00446-7.
3. Paci, G., Caria, J. & Lemke, E. A. Cargo transport through the nuclear pore complex at a glance. *J. Cell Sci.* **134**, jcs247874 (2021).
4. Paci, G., Zheng, T., Caria, J., Zilman, A. & Lemke, E. A. Molecular determinants of large cargo transport into the nucleus. *Elife* **9**, e55963 (2020).
5. Enam, C., Geffen, Y., Ravid, T. & Gardner, R. G. Protein Quality Control Degradation in the Nucleus. *Annu. Rev. Biochem.* **87**, 725–749 (2018).
6. Pack, C.-G. *et al.* Quantitative live-cell imaging reveals spatio-temporal dynamics and cytoplasmic assembly of the 26S proteasome. *Nat. Commun.* **5**, 3396 (5/2014).
7. Rock, K. L. *et al.* Inhibitors of the Proteasome Block the Degradation of Most Cell Proteins and the Generation of Peptides Presented on MHC Class I Molecules. *Cell* **78**, 761–771 (1994).
8. de Almeida, M. *et al.* AKIRIN2 controls the nuclear import of proteasomes in vertebrates. *Nature* **599**, 491–496 (2021).
9. Schraivogel, D. *et al.* High-speed fluorescence image–enabled cell sorting. *Science* **375**, 315–320 (2022).
10. Padavannil, A. *et al.* Importin-9 wraps around the H2A-H2B core to act as nuclear importer and histone chaperone. *Elife* **8**, e43630 (2019).
11. Nederlof, P. M., Wang, H.-R. & Baumeister, W. Nuclear localization signals of human and Thermoplasma proteasomal a subunits are functional in vitro. *Cell Biology* 5 (1995).
12. Monecke, T., Dickmanns, A. & Ficner, R. Allosteric control of the exportin CRM1 unraveled by crystal structure analysis. *FEBS J.* **281**, 4179–4194 (2014).
13. Bischoff, F. R., Klebe, C., Kretschmer, J., Wittinghofer, A. & Ponstingl, H. RanGAP1 induces GTPase activity of nuclear Ras-related Ran. *Proc. Natl. Acad. Sci. U. S. A.* **91**, 2587–2591 (1994).
14. Gu, X. *et al.* The midnolin-proteasome pathway catches proteins for ubiquitination-independent degradation. *Science* **381**, eadh5021 (2023).
15. Yang, R. *et al.* Structural basis for nuclear import of hepatitis B virus (HBV) nucleocapsid core. *Sci Adv* **10**, eadi7606 (2024).
16. Budenholzer, L., Breckel, C., Hickey, C. M. & Hochstrasser, M. The Sts1 nuclear import adaptor uses a noncanonical bipartite NLS and is directly degraded by the proteasome. *J. Cell Sci.* jcs.236158 (2020).
17. Chen, L. *et al.* Sts1 Plays a Key Role in Targeting Proteasomes to the Nucleus. *J. Biol. Chem.* **286**, 3104–3118 (01/2011).
18. Monda, J. K. *et al.* HAPSTR1 localizes HUWE1 to the nucleus to limit stress signaling pathways. *bioRxiv* 2023.01.26.525555 (2023) doi:10.1101/2023.01.26.525555.
19. Körner, M. *et al.* The FAM104 proteins VCF1/2 promote the nuclear localization of p97/VCP. *Elife* **12**, (2023).
20. Sallis, S. *et al.* The CHARGE syndrome-associated protein FAM172A controls AGO2 nuclear import. *Life Sci Alliance* **6**, (2023).
21. Enenkel, C., Kang, R. W., Wilfling, F. & Ernst, O. P. Intracellular localization of the proteasome in response to stress conditions. *J. Biol. Chem.* **298**, 102083 (2022).
22. Yasuda, S. *et al.* Stress- and ubiquitylation-dependent phase separation of the proteasome. *Nature* **578**, 296–300 (2020).
23. Kito, Y. *et al.* Cell cycle–dependent localization of the proteasome to chromatin. *Sci. Rep.* **10**, 5801 (12/2020).
24. Michlits, G. *et al.* Multilayered VBC score predicts sgRNAs that efficiently generate loss-of-function alleles. *Nat. Methods* **17**, 708–716 (2020).
25. Toste Rêgo, A. & da Fonseca, P. C. A. Characterization of Fully Recombinant Human 20S and 20S-PA200 Proteasome Complexes. *Mol. Cell* **76**, 138-147.e5 (10/2019).
26. Hodáková, Z. *et al.* Cryo-EM structure of the chain-elongating E3 ubiquitin ligase UBR5. *EMBO J.* **42**, e113348 (2023).
27. Weis, K., Mattaj, I. W. & Lamond, A. I. Identification of hSRP1 alpha as a functional receptor for nuclear localization sequences. *Science* **268**, 1049–1053 (1995).
28. Güttler, T. *et al.* NES consensus redefined by structures of PKI-type and Rev-type nuclear export signals bound to CRM1. *Nat. Struct. Mol. Biol.* **17**, 1367–1376 (2010).
29. Dorfer, V. *et al.* MS Amanda, a universal identification algorithm optimized for high accuracy tandem mass spectra. *J. Proteome Res.* **13**, 3679–3684 (2014).
30. Käll, L., Canterbury, J. D., Weston, J., Noble, W. S. & MacCoss, M. J. Semi-supervised learning for peptide identification from shotgun proteomics datasets. *Nat. Methods* **4**, 923–925 (2007).
31. Taus, T. *et al.* Universal and confident phosphorylation site localization using phosphoRS. *J. Proteome Res.* **10**, 5354–5362 (2011).
32. Doblmann, J. *et al.* ApQuant: Accurate label-free quantification by quality filtering. *J. Proteome Res.* **18**, 535–541 (2019).
33. Schwanhäusser, B. *et al.* Global quantification of mammalian gene expression control. *Nature* **473**, 337–342 (2011).
34. Punjani, A., Rubinstein, J. L., Fleet, D. J. & Brubaker, M. A. cryoSPARC: algorithms for rapid unsupervised cryo-EM structure determination. *Nat. Methods* **14**, 290–296 (2017).

35. Adolf, F. *et al.* Visualizing chaperone-mediated multistep assembly of the human 20S proteasome. *Nat. Struct. Mol. Biol.* 1–13 (2024).
36. Asarnow, D., Palovcak, E. & Cheng, Y. *Asarnow/Pyem: UCSF Pyem v0.5*. (Zenodo, 2019). doi:10.5281/ZENODO.3576630.
37. Kimanius, D., Dong, L., Sharov, G., Nakane, T. & Scheres, S. H. W. New tools for automated cryo-EM single-particle analysis in RELION-4.0. *Biochem. J.* **478**, 4169–4185 (2021).
38. Kimanius, D. *et al.* Data-driven regularization lowers the size barrier of cryo-EM structure determination. *Nat. Methods* 1–6 (2024).
39. Sanchez-Garcia, R. *et al.* DeepEMhancer: a deep learning solution for cryo-EM volume post-processing. *Commun. Biol.* **4**, 874 (2021).
40. Wagner, T. *et al.* SPHIRE-crYOLO is a fast and accurate fully automated particle picker for cryo-EM. *Commun. Biol.* **2**, 218 (2019).
41. Jumper, J. *et al.* Highly accurate protein structure prediction with AlphaFold. *Nature* **596**, 583–589 (2021).
42. Meng, E. C. *et al.* UCSF ChimeraX: Tools for structure building and analysis. *Protein Sci.* **32**, e4792 (2023).
43. Pettersen, E. F. *et al.* UCSF ChimeraX: Structure visualization for researchers, educators, and developers. *Protein Sci.* **30**, 70–82 (2021).
44. Kidmose, R. T. *et al.* Namdinator - automatic molecular dynamics flexible fitting of structural models into cryo-EM and crystallography experimental maps. *IUCrJ* **6**, 526–531 (2019).
45. Croll, T. I. ISOLDE: a physically realistic environment for model building into low-resolution electron-density maps. *Acta Crystallogr. D Struct. Biol.* **74**, 519–530 (2018).
46. Croll, T. I. & Andersen, G. R. Re-evaluation of low-resolution crystal structures via interactive molecular-dynamics flexible fitting (iMDFF): a case study in complement C4. *Acta Crystallogr. D Struct. Biol.* **72**, 1006–1016 (2016).
47. Emsley, P. & Cowtan, K. *Coot* : model-building tools for molecular graphics. *Acta Crystallogr. D Biol. Crystallogr.* **60**, 2126–2132 (2004).
48. Emsley, P., Lohkamp, B., Scott, W. G. & Cowtan, K. Features and development of coot. *Acta Crystallogr. D Biol. Crystallogr.* **66**, 486–501 (2010).
49. Davis, I. W. *et al.* MolProbity: all-atom contacts and structure validation for proteins and nucleic acids. *Nucleic Acids Res.* **35**, W375-83 (2007).
50. Williams, C. J. *et al.* MolProbity: More and better reference data for improved all-atom structure validation. *Protein Sci.* **27**, 293–315 (2018).
51. Afonine, P. V. *et al.* New tools for the analysis and validation of cryo-EM maps and atomic models. *Acta Crystallogr. D Struct. Biol.* **74**, 814–840 (2018).
52. Afonine, P. V. *et al.* Real-space refinement in PHENIX for cryo-EM and crystallography. *Acta Crystallogr. D Struct. Biol.* **74**, 531–544 (2018).
53. Wang, R. Y.-R. *et al.* Automated structure refinement of macromolecular assemblies from cryo-EM maps using Rosetta. *Elife* **5**, (2016).
54. Schindelin, J. *et al.* Fiji: an open-source platform for biological-image analysis. *Nat. Methods* **9**, 676–682 (2012).
55. Stringer, C., Wang, T., Michaelos, M. & Pachitariu, M. Cellpose: a generalist algorithm for cellular segmentation. *Nat. Methods* **18**, 100–106 (2021).

Acknowledgements

We thank all members of the Haselbach and Zuber group for their great support and scientific discussions, the Electron Microscopy facility of the Vienna BioCenter, in particular Thomas Heuser; Victor-Valentin Hodirnau at Institute of Science and Technology Austria EM facility for cryo-EM data collection. We are thankful to the Peters, Plaschka and Clausen group for sharing chemicals and lab equipment. This work was further supported by Vienna Biocenter Core Facilities: the Light Microscopy Facility at Vienna BioCenter Core Facilities (VBCF) and the IMP/IMB/GMI BioOptics Facilty, in particular Thomas Leindl and Pawel Pasierbek; by the Protein Technologies Facility at the Vienna BioCenter Core Facilities (VBCF), in particular Arthur Sedivy; and Proteomics analyses were performed by the Proteomics Facility at IMP/IMBA/GMI using the VBCF instrument pool, in particular Otto Hudecz and Ines Steinmacher. We gratefully thank Alexander Schleiffer and Thomas Burkard for evolutionary conservation analysis; Dilantha Perera and Marius Pörschke for their help with nuclear import assays; Achim Dickmanns, Julian Ehrmann, and Ulrich Hohmann for providing purified proteins. We also thank Maximilian Spicer and Milka Kostic (Life Science Editors).

Funding
European Union's Framework Programme for Research and Innovation Horizon 2020 (2014-2020) (ZH)
Marie Curie Skłodowska Grant Agreement Nr. 847548 (ZH)
FWF SFB F79 targeted protein degradation (HLB)
Boehringer Ingelheim (HLB, Haselbach lab)

Author contributions
Conceptualization: HLB, RWK, JZ, DH
Methodology: HLB, RWK, LEG, ZH, ZK, IG, MA, MH, SH, FA, HK, AD, SCH, JZ, DH
Investigation: HLB, RWK, LEG
Visualization: HLB, RWK, LEG
Funding acquisition: DH
Project administration: DH
Supervision: DH, JZ
Writing – original draft: HLB, RWK
Writing – review & editing: HLB, RWK, DH, JZ, ZH

Competing interests:
J.Z. is a founder, shareholder and scientific advisor of Quantro Therapeutics. J.Z., D.H. and the Zuber and Haselbach laboratories receive research support and funding from Boehringer Ingelheim.

Data and material availability
Atomic coordinates and cryo-EM density maps have been deposited in the Protein Data Bank (PDB) under accession codes PDB: <xx> (<link >), and EMD-<xx> (<link>). The raw micrographs were submitted to the EMPIAR database under accession code EMPIAR-
<xx> <link>). Mass spectrometry datasets have been uploaded to PRoteomics IDEntifications Database (PRIDE) under project accession: PXD052012. Other source data are included as attachments to the manuscript.

Extended Data

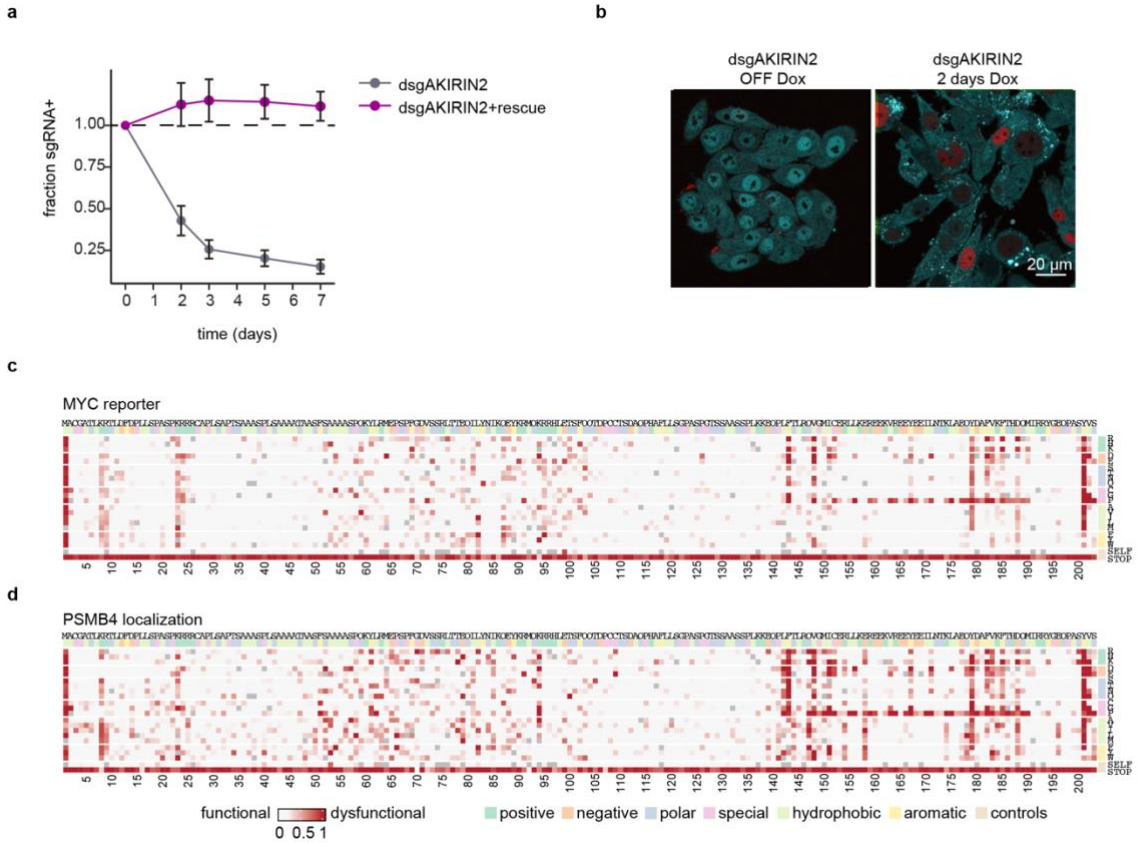

Extended Data Fig. 1 | Generation of the 20S reporter cell line for the SMScreens and the individual results of the FACS readouts. a, Validation of the AKIRIN2 knockout and a rescue construct in the 20S reporter cell line with either only dsgRNA against endogenous AKIRIN2 or additionally expressing a wildtype rescue construct. (Competition assay analysing sgRNA+ cells by FACS (staining against hCD2) after 2, 3, 5, or 7 days of KO induction. **b**, Confocal microscopy images imaging the localisation of StayGold-labelled proteasomes as well as mCherry-MYC after 2 days of AKIRIN2 knockout. **c**,**d**, Individual heat plots of the SMScreens readouts of either (**c**) mCherry-MYC FACS based readout, sorting 1-2% of the cells with high mCherry signal after 2-4 days upon KO of endogenous AKIRIN2, or (**d**) Image-based FACS readout of 5% of the cells that show a low correlation of StayGold-labelled proteasomes with the nuclear marker DraQ5 after 2-4 days of KO induction.

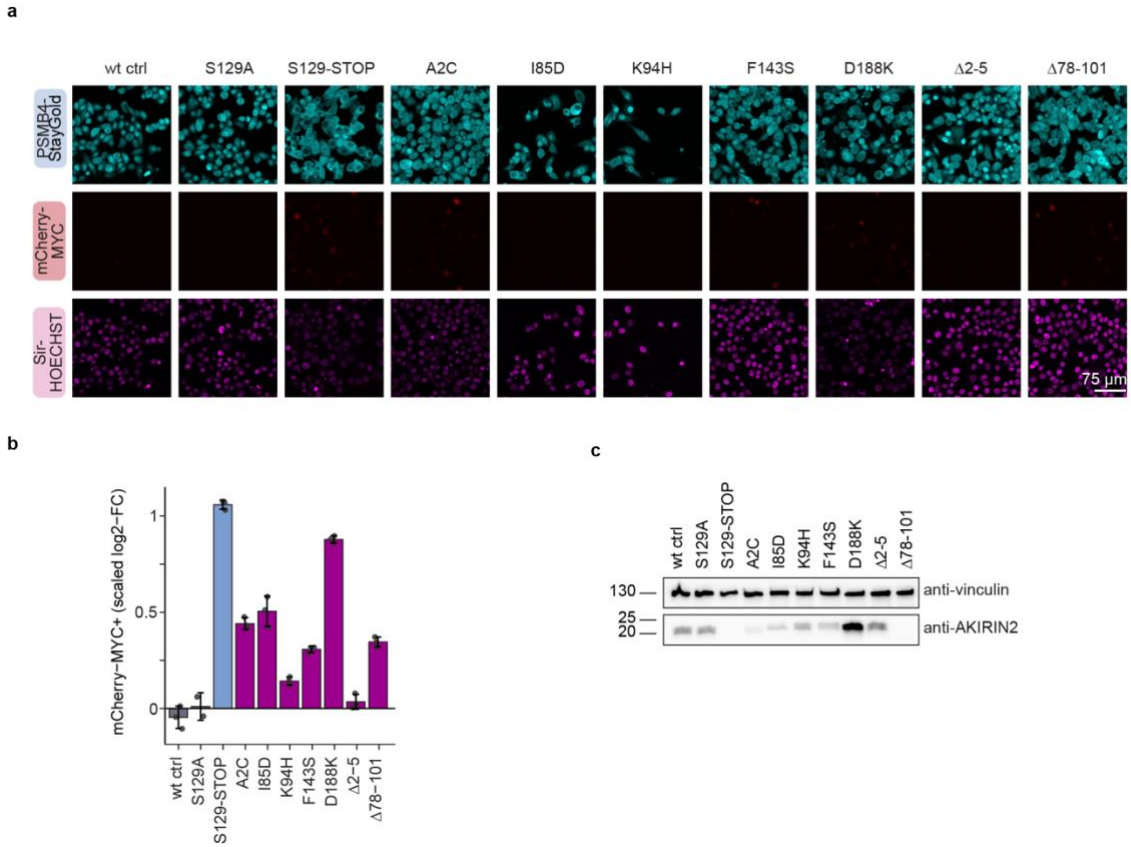

Extended Data Fig. 2 | Analysis of individual validation mutants. a, Confocal microscopy images of individual point mutations and deletion mutants after 2 days of KO induction. **b**, FACS analysis of mCherry-MYC after 2-3 days of KO induction. **c**, Western Blot analysis of AKIRIN2 levels of the individual mutants after 3 days of KO induction.

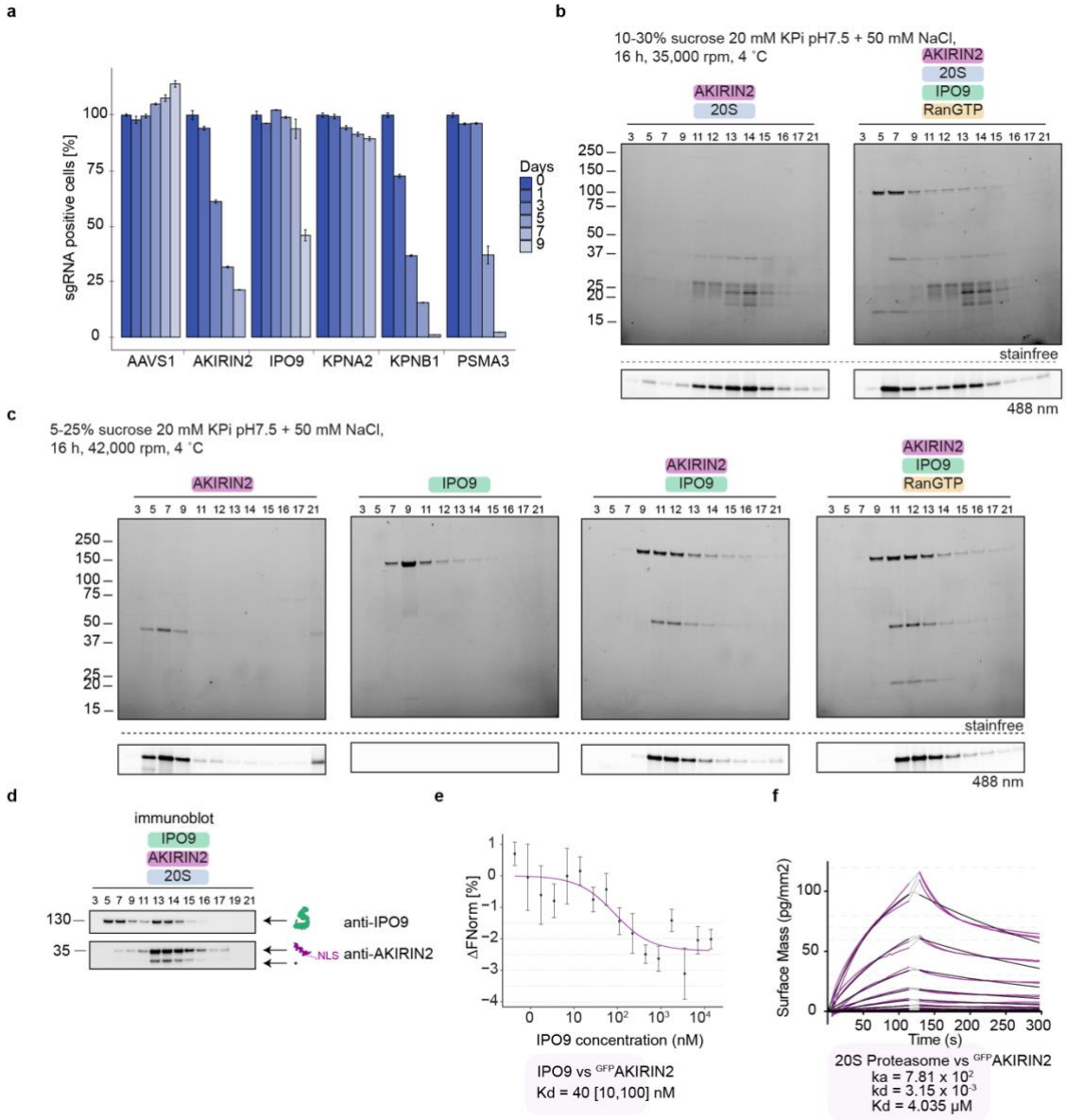

Extended Data Fig. 3 | 20S:AKIRIN2:IPO9 reconstitution. a, Competitive profiling assay of sgAAVS1, sgAKIRIN2, sgIPO9, or sgPSMB3 up to 9 days after knockout induction. Data are normalized to day 0 and are presented as mean ± s.d. **b**, 10-30% sucrose, 35,00 rpm for 16 h, including 20S, IPO9, AKIRIN2 and RanGTP. **c**, 5-25% sucrose gradient, 42,000 rpm for 16 h, including IPO9, AKIRIN2 and RanGTP. (**a**,**b**) Showing stainfree gels as well as 488 nm imaged gels to visualize GFP-AKIRIN2. **d**, Western blot of the SDS-PAGE gel analysing individual fractions of a sucrose density gradient reconstituting the complex 20S:AKIRIN2:IPO9 blotting against AKIRIN2 and IPO9, *AKIRIN2 shows a double band if the samples are not cooked before loading on SDS-PAGE which is likely the not fully denaturated GFP-tag which allows us to image GFP in the SDS-PAGE gel. **e**, MST binding curve for IPO9 and AKIRIN2. **f**, GCI binding curves for proteasomes and AKIRIN2.

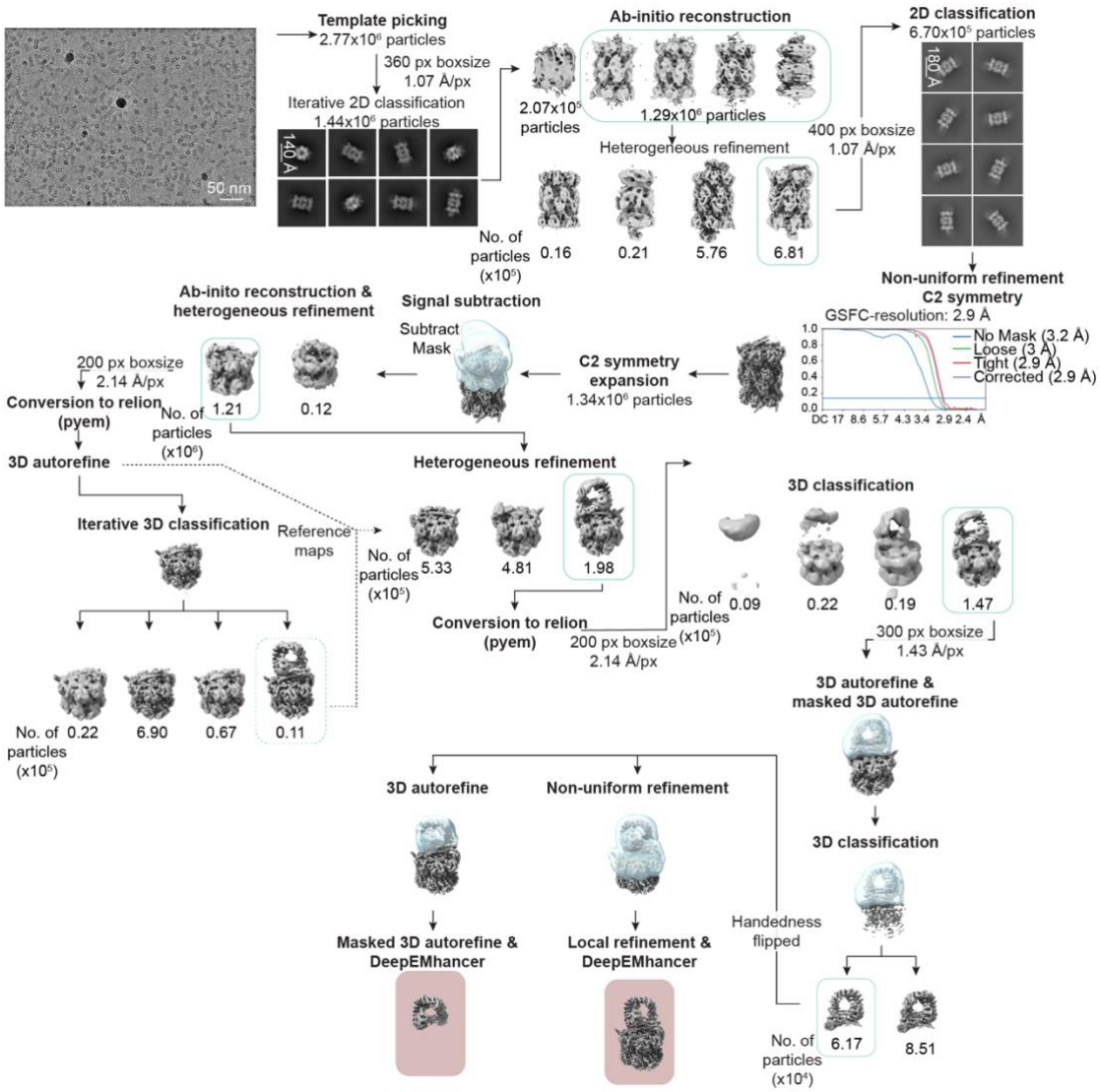

Extended Data Fig. 4 | Processing pipeline for the ternary complex 20S:AKIRIN2:IPO9. Workflow for the single particle analysis of the 20S:AKIRIN2:IPO9 dataset. Analysis was performed in cryoSPARC and relion. Green outlines indicate selected particles and maps, when selected from multiple classes, for downstream refinements. Final maps are indicated by a red box. See the methods section for a more detailed description.

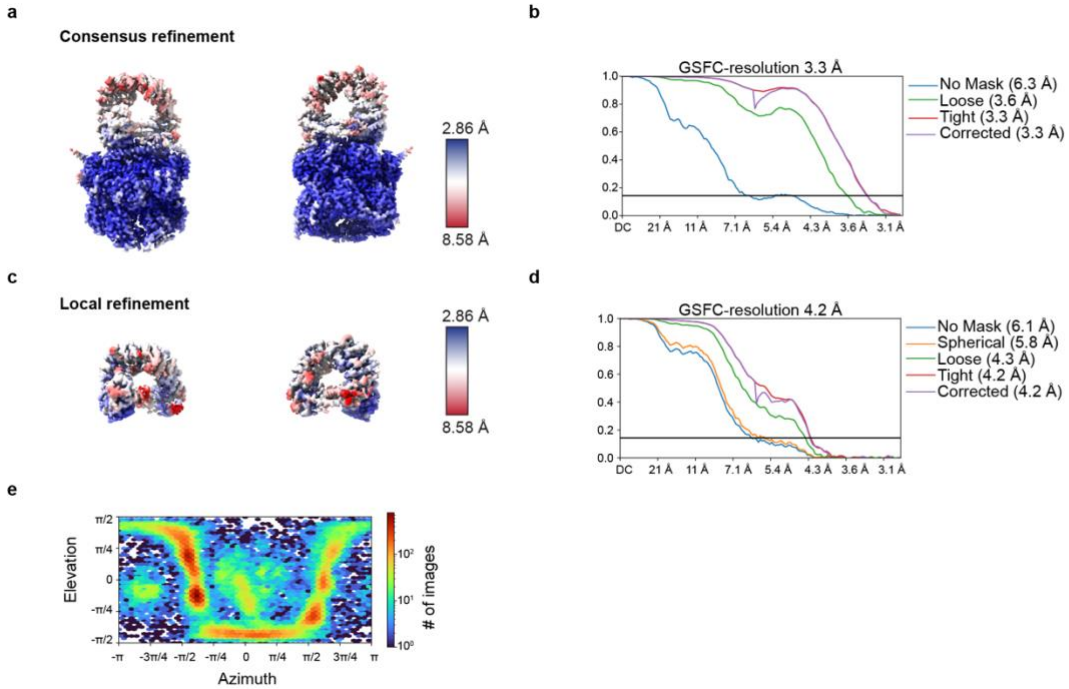

Extended Data Fig. 5 | 20S:AKIRIN2:IPO9 reconstructions.
CryoEM reconstructions of the 20S:AKIRIN2:IPO9 dataset. **a**, DeepEMhanced map of the consensus refinement and **b**, GSFC curve for global resolution estimation. **c**, DeepEMhanced map of the local refinement and **d**, GSFC curve for global resolution estimation created in cryoSPARC using the half maps of the final relion refinement. **e**, Viewing angle distribution as a heat plot.

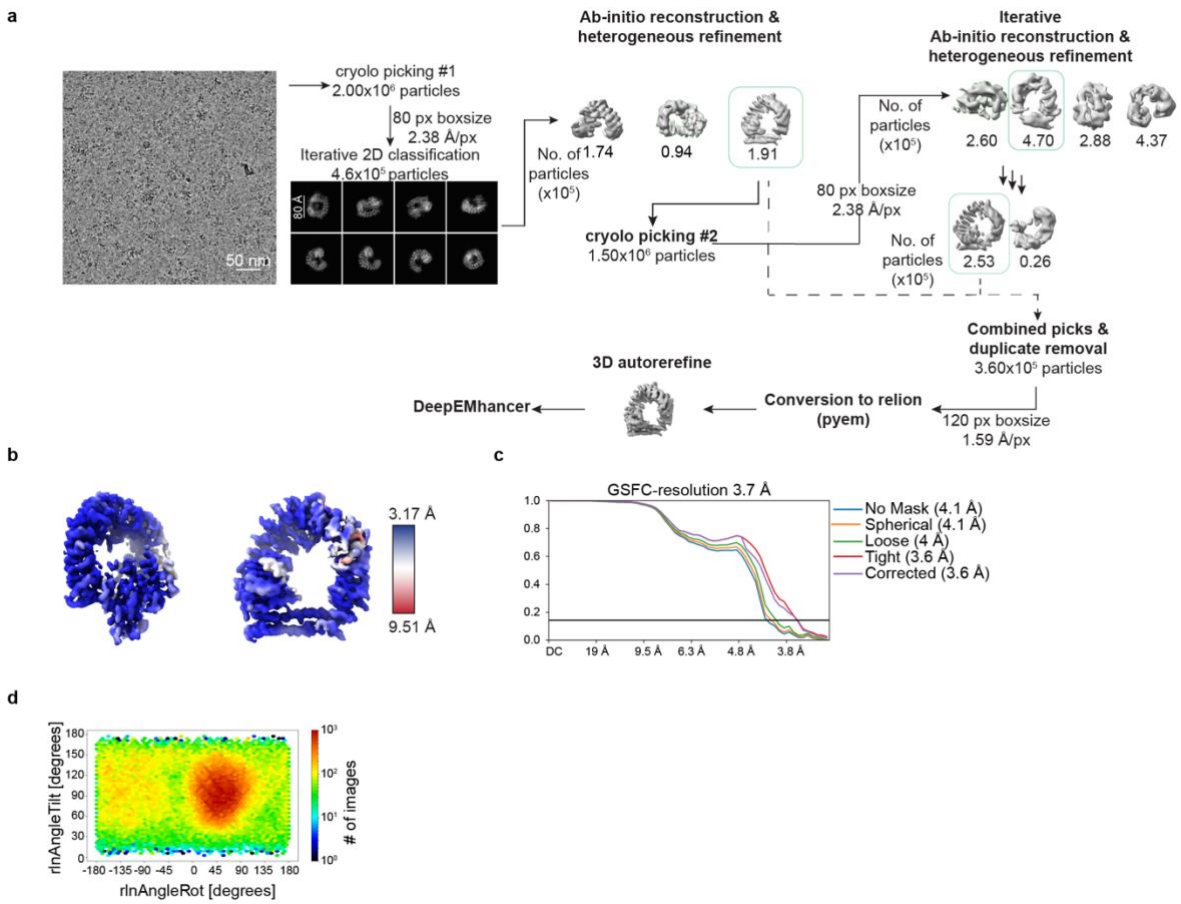

Extended Data Fig. 6 | Processing pipeline for the binary complex IPO9:AKIRIN2.
Single particle analysis of the IPO9:AKIRIN2 dataset. **a**, Analysis was performed in cryoSPARC and relion. Green outlines indicate selected particles and maps selected after classification jobs. See the methods section for a more detailed description. **b**, DeepEMhanced cryoEM map of the IPO9:AKIRIN2 complex coloured by local resolution. **c**, GSFC curve for global resolution estimation created in cryoSPARC using the half maps of the final relion refinement. **d**, Viewing angle distribution plot.

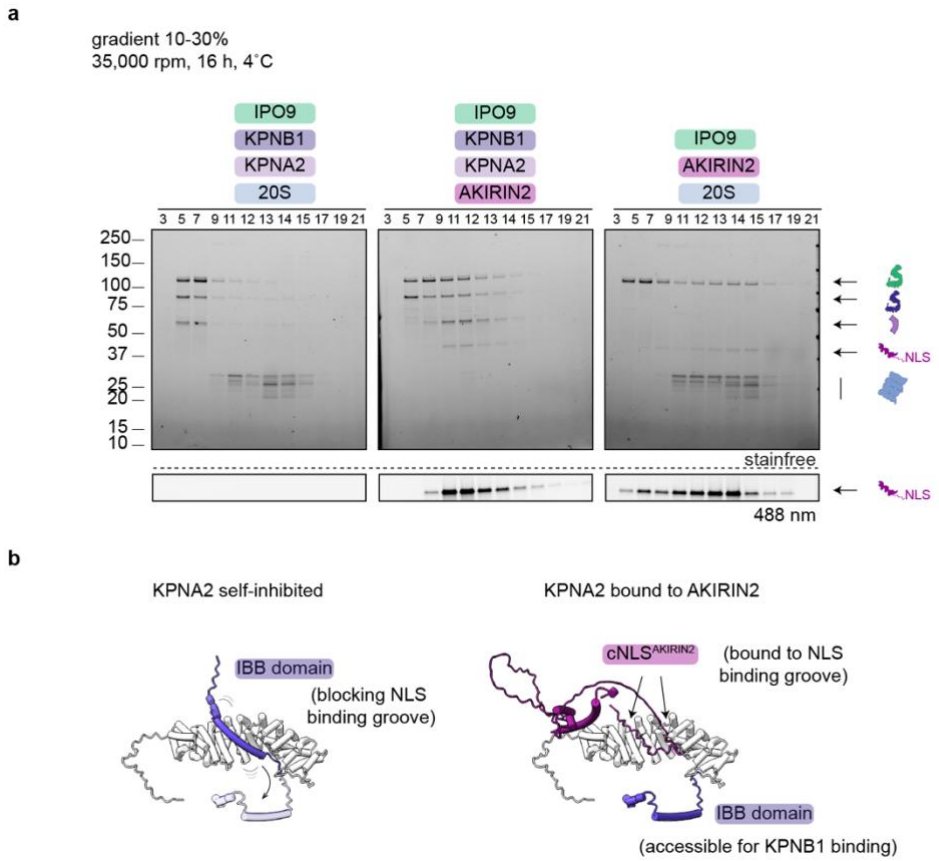

Extended Data Fig. 7 | Reconstitution of the import complexes.
a, SDS-PAGE gels analysing individual fractions of sucrose density gradients of reconstituted subcomplexes. Showing stainfree gels as well as 488 nm imaged gels to visualize GFP-AKIRIN2. **b**, AF2 prediction of KPNA2 solely or together with AKIRIN2 (pink) showing displacement of the self-inhibitory IBB domain (purple) of KPNA2 in the presence of AKIRIN2. Bipartite NLS of AKIRIN2 binds into minor and major binding groove of KPNA2.

Supplementary table 1: CryoEM experimental table

	ternary complex 20S:AKIRIN2:IPO9			binary complex IPO9:AKIRIN2
	Consensus refinement	Local refinement	Composite structure	
	(EMDB-xxxx)	(EMD-xxxx)	(EMD-xxxx)	(EMDB-xxxx)
	(PDB xxxx)	(PDB-xxxx)	(PDB-xxxx)	(PDB xxxx)
Data collection and processing				
Magnification	81,000 x			130,000 x
Voltage (kV)	300			300
Electron exposure (e–/Åˆ2)	44,4			40
Detector	Gatan K3 BioQuantum			Falcon 4/4i
Defocus range (μm)	-1.0 to -1.9 μm (0.2 increments)			-1.0 to 2.0 μm (0.25 increments)
Pixel size (Å)	1.07			0.952
Adjusted Pixel size (Å)	1.055			0.952
Final map pixel size (Å)	1.407			1.585
Symmetry imposed	C1			C1
Initial particle images (no.)	1,774,967			1,995,239
Final particle images (no.)	61,74			360,044
Map resolution (Å)	3.3	4.2	N.A.	3.7
FSC threshold	0.143		N.A.	0.143
Map resolution range (Å)	3.2-8.3	3.6-9.3	N.A.	3.6-5.7
Refinement				
Initial model used (PDB code)	PDB-7NHT, AF2			AF2
Model resolution (Å)	3.4	4.4	3.5	4.5
FSC threshold	0.5			0.5
Map sharpening *B* factor (Åˆ2)	60.1	115.1	N.A.	189.4
Model composition				
Non-hydrogen atoms	16542	3968	20510	6492
Protein residues	2120	747	2867	1083
Ligands	0	0	0	0

B factors (Å^2) min/max/mean	43.23/164.34/80.69	82.04/232.18/123.14	13.85/93.41/41.02	72.9 / 229.0 / 111.7
R.m.s. deviations				
Bond lengths (Å)	0.003	0.002	0.003	0.016
Bond angles (°)	0.555	0.534	0.535	1.9
Validation				
MolProbity score	1.49	1.54	1.75	0.69
Clashscore	4.50	5.10	5.21	0.55
Poor rotamers (%)	1.77	N.A.	2.66	N.A.
Ramachandran plot				
Favored (%)	97.7	96.1	97.2	98.5
Allowed (%)	2.3	3.92	2.8	1.4
Disallowed (%)	0.0	0.0	0.0	0.09

Supplementary table 2: Used guide RNAs

Target/name	Sequence
AKIRIN2-1	GCCGGGTCCCACCTGTGGTG
AKIRIN2-1	GCGGCCGCCGACAACGGGG
IPO9-1	GTTAGGGTGTTCCAAACAAT
IPO9-2	GTTAGGGTGTTCCAAACAAT
KPNA2-1	GATGCAGGAGCCGAACTA
KPNA2-2	GATGGTCCAAATGAACGAAT
KPNB1	GAGCTCCTAGAGACTACAGAC
AAVS1-1	GCTGTGCCCCGATGCACAC
AAVS1-2	GCTTGGCAAACTCACTCTT

Supplementary video 1: Ternary structure of 20S:AKIRIN2:IPO9 showing full 20S matched with publish pdb model (source: pdb 6RGQ). Close-ups of binding interfaces between AKIRIN2 and IPO9 as well as AKIRIN2 and alpha subunits of the 20S.

Supplementary video 2: Conformational change of IPO9 in the dimeric structure bound to one dimer of AKIRIN2 from a closed conformation to an open conformation when engaged with a second AKIRIN2 dimer and the proteasome.